

SQUEEZE CASTING
OF
Zn-Bi MONOTECTIC ALLOY

by

Hakan Erturan

B.S. in Mechanical Sciences, Naval Academy, 1988

Submitted to the Institute for Graduate Studies in
Science and Engineering in partial fulfillment of
the requirements for the degree of
Master of Science
in
Defence Technology Program
Mechanical Sciences Option

Bogazici University Library



39001100120230

14

Boğaziçi University

June, 1994

ACKNOWLEDGMENTS

I wish to thank to Assoc. Prof. Mahmut A. Savaş, my thesis supervisor, for his invaluable help and patience and, also to Prof. Sabri Altıntaş for his support and interest during this study.

I also wish to thank to research assistants Metin Yılmaz and Hakan Gökbayrak for their support and help in the experimental work and, to Information Ltd. and Mr. Selim Can for providing their facilities during typing this thesis.

Finally, I wish to thank to my family and my friends for their moral support during this work.

ABSTRACT

Zn- 1.9 wt.% Bi monotectic alloy was squeeze cast under pressures of 50, 85 and 120 MPa at a constant die temperature of 250 °C. The same die was used also for the gravity cast specimens of the same alloy. For comparison purposes the pure zinc castings were gravity cast and squeeze cast under 120 MPa at a die temperature of 400 °C.

It was found that the porosity level in the castings were decreased with the application of squeezing pressure which resulted in an increase in tensile strength and hardness values. However, the microstructural examination showed that the segregation tendency of bismuth phase along the centerline was increased with increasing pressure and caused an inhomogeneous distribution of bismuth phase in the radial direction. The distribution of bismuth phase was also inhomogeneous in the longitudinal direction due to gravitational segregation.

In the macrostructural examination of the samples, the average grain size was found to decrease as the squeezing pressure was increased. A variation in grain size along longitudinal axis of the specimens was also observed. The grains were coarser near the bottom end and were finer near the punch end of castings. It appears that the lower part of the castings were solidified before pressure application.

ÖZET

Bu çalışmada yüksek saflıktaki çinko ve bizmuttan ağırlık olarak % 1.9 bizmut fazı içeren monotektik alaşımı hazırlanmıştır. Bu alaşımdan 50, 85 ve 120 MPa basınçlar altında, 250 °C sabit kalıp sıcaklığında sıkıştırma döküm yöntemi ile numuneler üretilmiştir. Ayrıca, bir karşılaştırma yapmak üzere aynı alaşımdan sıkıştırılmadan 20 °C ve 250 °C kalıp sıcaklıklarında, saf çinkodan ise 400 °C sıcaklığındaki kalıplara dökümler yapılmıştır.

Basıncın artması ile birlikte dökümlerdeki boşluk miktarında bir düşme görülmüş ve bunun sonucunda dökümlerin çekme dayanımı ve sertlik özelliklerinde iyileşmeler gözlenmiştir. Ancak geç katılaşılan bizmut yönünden zengin sıvı faz artan basınçla birlikte dökümün merkezine doğru itildiğinden döküm içyapısında radyal yönde bizmut taneciklerinin düzgün olmayan bir dağılım gösterdiği gözlenmiştir. Ayrıca, daha ağır olan bizmut fazı dökümün alt kısımlarına doğru indiğinden aksenal yönde de düzgün bir dağılım gözlenmemiştir.

Dökümlerde yapılan makro yapı incelemelerinde ortalama tane boyutunun basıncın artması ile birlikte küçüldüğü görülmüştür. Ek olarak, tane boyutları aksenal yönde de farklılık göstermiştir. Ortalama tane boyutu zimbaya yakın kısımlarda küçülürken, dökümün alt kısımlarında büyümüştür. Bu farklılığın dökümün alt kısımlarının basınç uygulanmadan önce katılaşıp olması nedeniyle ortaya çıktığı anlaşılmaktadır.

TABLE OF CONTENTS

ACKNOWLEDGMENTS.....	iii
ABSTRACT.....	iv
ÖZET.....	v
LIST OF FIGURES.....	viii
LIST OF TABLES.....	xi
LIST OF SYMBOLS.....	xii
I. INTRODUCTION.....	1
II. LITERATURE REVIEW.....	3
2.1. Squeeze Casting Method.....	3
2.1.1. Melt Quality and Quantity.....	8
2.1.2. Equipment and Tooling.....	9
2.1.3. Casting Temperature.....	11
2.1.4. Tooling Temperature.....	12
2.1.5. Time Delay Before Pressure Application.....	12
2.1.6. Lubrication.....	12
2.1.7 Pressure Level and Duration.....	13
2.2. Application of Squeeze Casting in Metal Matrix Composites.....	15
2.3. Comparison of Squeeze Casting Method with Other Methods.....	21
2.4. Monotectic Solidificaton.....	27
2.4.1. Monotectic Phase Diagram.....	27
2.4.2. Normal (Bulk) Monotectic Freezing.....	29
2.4.3. Progressive, or Steady State. MonotecticFreezing.....	30
2.5. The Zn-Bi System.....	35
2.6. Squeeze Casting of Monotectic Alloys.....	39
III. EXPERIMENTAL STUDY.....	41
3.1. Dies and Materials Used.....	41
3.2. Melting and Casting Practise.....	41
3.2.1. Preparation of Castings.....	41

3.2.2. Squeeze Casting.....	43
3.3. Cooling Curve Determination.....	45
3.4. Chip Length Measurement.....	46
3.5. Tensile Testing.....	47
3.6. Density Measurement.....	47
3.7. Optical Metallography.....	49
3.7.1. Macrostructure Examination.....	49
3.7.2. Microstructure Examination.....	49
3.8. Hardness Test.....	49
IV. RESULTS AND DISCUSSION.....	50
4.1. Effects of Pressure on the Cooling Rates of Castings.....	50
4.2. Effects of Pressure on Macro- and Microstructures	50
4.2.1 Macrostructure.....	50
4.2.2. Microstructure.....	55
4.3. Chip Length Variation.....	59
4.4. Tensile Properties.....	61
4.5. Hardness Variation.....	65
4.6. Macro and Microstructures vs Mechanical Properties.....	67
V. CONCLUSIONS.....	69
VI. RECOMMENDATIONS FOR FUTURE WORK	71
VII. REFERENCES.....	72

LIST OF FIGURES

		Page
Fig. 2.1	Tooling and processing sequence for squeeze casting [11].	4
Fig. 2.2	Production of solid ingot and hollow shapes by direct squeeze casting process [15].	5
Fig. 2.3	The squeeze forming process and associated tooling design for the production of a vehicle wheel [17].	6
Fig. 2.4	Ube vertical shot indirect squeeze casting system [15].	7
Fig. 2.5	Two different squeeze casting die designs for the same shape [12].	10
Fig. 2.6	Relation between mechanical properties and section thickness (a) for design A, (b) for design B [12].	11
Fig. 2.7	Movement of liquid metal through parallel fiber bundles (a) wetting system, (b) non-wetting system [19].	15
Fig. 2.8	Infiltration of (a) a wedge, (b) the contact area between two fibers or spherical particles by a non-wetting metal [20].	19
Fig. 2.9	Melt and die temperatures versus time for monolithic A357 during, (a) gravity die casting and, (b) squeeze casting at 100 MPa [8].	20
Fig. 2.10	Mechanical properties of squeeze cast and fully heat treated AZ91 as a function of casting process [15].	22
Fig. 2.11	Variation of fracture tensile strength and fracture strain with squeezing pressure in Al-7%Si alloy [21].	23
Fig. 2.12	Variation of impact toughness with squeezing pressure in Al-7%Si alloy [21].	24
Fig. 2.13	Fatigue curves for diesel engine pistons (E332-T5 Al) produced by squeeze casting and gravity die casting [11].	24
Fig. 2.14	Squeeze casting rating and potential automotive applications [11].	25
Fig. 2.15	Typical monotectic equilibrium diagram [22].	28
Fig. 2.16	Schematic drawing of unidirectional freezing of an alloy of monotectic composition with freezing from bottom to top showing initial deposition of α -phase [22].	31

- Fig. 2.17 The nucleation behavior of liquid L_2 (a) non-wetting, (b) partial wetting, (c) complete wetting [22]. 31
- Fig. 2.18 Schematic drawing of unidirectional growth of the monotectic alloy [22]. 33
- Fig. 2.19 Diagrammatic illustration showing how growth front oscillations combined with post solidification effects caused degeneration of a rod-like composite into an aligned droplet array [25]. 36
- Fig. 2.20 Equilibrium phase diagram of Zn-Bi system [29]. 37
- Fig. 2.21 Variation of free energy per mol as a function of composition (X_{Zn}) at 500 °K: (a) solid solution (G_S), (b) liquid solution (G_L) [29]. 37
- Fig. 2.22 Phase diagram of Zn-Bi system, showing metastable extension of liquid phase field (binodal), liquid spinodal and T_O of liquid and solid solution at Zn-rich end [29]. 38
- Fig. 2.23 Microstructures of Zn-Bi alloys, (a) $X_{Zn}=0.03$, (b) $X_{Zn}=0.07$, (c) $X_{Zn}=0.09$, (d) $X_{Zn}=0.17$ [6]. 39
- Fig. 3.1 Squeeze casting die used for the production of the castings. 42
- Fig. 3.2 Squeeze casting die used in determination of cooling curves. 42
- Fig. 3.3 Squeeze casting set-up. 44
- Fig. 3.4 Castings produced by gravity casting and squeeze casting. 44
- Fig. 3.5 Schematic representation of the experimental set-up used in cooling curve determination. 45
- Fig. 3.6 An enlarged view of the chip resulted from the machining of a squeeze cast Zn-Bi monotectic alloy. 47
- Fig. 3.7 Tension test specimen (a) dimensions, (b) actual view. 48
- Fig. 4.1 Cooling curves recorded from the melt at the die center-line location during squeeze casting and gravity casting. 51
- Fig. 4.2 Cooling curves for the melt-die interface during squeeze casting and gravity casting. 51
- Fig. 4.3 Cooling curves for the die during squeeze casting and gravity casting. 51
- Fig. 4.4 Macrostructures of not-squeezed specimens cast into (a) cold die at 20 °C, (b) hot die at 250 °C. 52

Fig. 4.5	Macrostructures of squeeze cast specimens squeezed under (a) 50 MPa, (b) 120 MPa.	53
Fig. 4.6	Average grain diameter as a function of casting condition.	54
Fig. 4.7	Change in grain size along the longitudinal cross-section of specimen squeeze cast under 120 MPa.	54
Fig. 4.8	Microstructure at the central part of a Zn-Bi monotectic specimen cast into cold die and not squeezed (x320).	55
Fig. 4.9	Microstructure of the same region under a higher magnification (x800, oil lens).	55
Fig. 4.10	Microstructure at the central part of a Zn-Bi monotectic specimen squeeze cast under 85 MPa (x320).	56
Fig. 4.11	Microstructure at the bottom end of the same specimen (x800, oil lens).	57
Fig. 4.12	Microstructure of the same specimen at top part (1.5 cm from the punch end) (x320)	57
Fig. 4.13	Microstructure of the same region of the Zn-Bi specimen squeeze cast under 85 MPa (x800, oil lens).	57
Fig. 4.14	Diagrammatic illustration proposed for the strain induced macro-segregation phenomena of Bi-rich phase in squeeze cast Zn-Bi monotectic alloy.	58
Fig. 4.15	Chips obtained from; (a) pure zinc not-squeezed, (b) pure zinc squeeze cast at 120 MPa, (c) Zn-Bi not-squeezed, (d) Zn-Bi squeeze cast at 120 MPa, castings at a cutting speed of 69 m/min	59
Fig. 4.16	The variation of average chip length in Zn-Bi monotectic alloy with squeezing pressure at a cutting speed of $V=23.4$ m/min.	60
Fig. 4.17	The variation of tensile strength with squeezing pressure.	62
Fig. 4.18	Effect of squeezing pressure on; (a) density, (b) porosity level.	63
Fig. 4.19	Variation of Vickers Hardness in Zn-Bi monotectic specimens; along centerlines of specimens.	66
Fig. 4.20	Variation of hardness in the radial direction of the specimen squeeze cast under 120 MPa.	66
Fig. 4.21	The relative position of the tension test specimen in a typical casting	67

LIST OF TABLES

	Page
Table 2.1 Stages in the squeeze forming process of the vehicle wheel given in Fig 2.3 [17].	6
Table 2.2 The practical applications of cast MMC's for commercial products in Japan [7].	16
Table 2.3 Comparative properties of commercial ferrous alloys [98].	22
Table 2.4 Comparative properties of JIS AC4C-T6 (356-T6) [98].	23
Table 2.5 Monotectic temperatures (T_m), height of miscibility gaps ($T_c - T_m$) and freezing ranges ($T_m - T_e$) of some monotectic systems [30].	38
Table 2.6 Effects of squeeze casting on the wide freezing range alloys [14].	40
Table 4.1 Average chip length vs alloy composition, squeezing pressure, die temperature and cutting speed.	60
Table 4.2 Tension test data.	61
Table 4.3 Apparent densities and porosity contents calculated in the tension test specimens.	63
Table 4.4 Tensile properties of gravity cast, squeeze cast and directionally solidified Zn-Bi monotectic alloy.	64
Table 4.5 Average Vickers Hardness values of specimens.	65

LIST OF SYMBOLS

C	Number of components
C_m	Monotectic composition
C_o	Composition
D	Density, Diameter
F	Number of degrees of freedom
G	Gibb's free energy
g	Gravitational acceleration
L	Liquid phase
P	Number of phases
r	Radius
T	Temperature
T_m	Monotectic temperature
α	Solid phase
ϵ_f	Elongation at fracture
γ	Interfacial energy
λ	Interfacial spacing, Wavelength
μ	Viscosity
θ	Wetting angle
$\sigma_{0.2}$	Yield Strength
σ_f	Fracture strength

I. INTRODUCTION

Relatively little attention has been given to monotectic alloys until recent years due to the difficulties in their production. Components of monotectic alloys are almost insoluble in each other and have very distinct physical, mechanical and thermal properties [1,2]. Phase separation due to different densities of the components and wide freezing ranges of the alloys and unsuitable interfacial energy relations between the phases are the most important problems faced in freezing of monotectic alloys. Experiments are still being carried on in space and under microgravity conditions to overcome these problems [2-6]. Although some improvements have been reported in in-situ composite production of monotectic alloys by directional solidification technique there are still problems to be solved. However, directional solidification method is rather expensive and is unsuitable for mass production.

Squeeze casting method has recently been in use for industrial applications especially, for the production of fiber or particulate reinforced metal matrix composites and, for the infiltration of fiber preforms with a non-wetting metal [7-10]. Squeeze casting method is also proved to improve the mechanical properties of ferrous and non-ferrous alloys [11-13] and wide freezing range binary alloys [11, 14].

Considerable interest has been expressed recently in monotectic systems. This interest has been based on predictions which state many alloys in monotectic systems may exhibit superconducting properties or high coercive magnetic field strength [3]. Monotectic alloys also contain industrially important materials such as free machining alloys based on Cu-Pb or Fe-Mn-S, or bearing alloys in the former [1]. Cu-Pb composite is also a promising battery grid material [4]. In the present

study Zn-Bi monotectic alloy has been chosen as a model system for monotectics for its relatively low critical and monotectic temperatures. The effects of pressure application on the mechanical and physical properties and, also on the macro- and microstructures of the castings have been investigated.

II. LITERATURE REVIEW

2.1. Squeeze Casting Method

Squeeze casting term is used to describe a combined metal forming process in which the pressure is applied to the metal in its semi-solid state to produce finished shapes. This process is also called as 'liquid metal forging', 'squeeze forming', 'extrusion casting' or 'pressure crystallization', because it is the combination of gravity die casting and closed die forging processes [11,12,15].

In this method solidification is accomplished under high pressure sufficient to prevent the appearance of either gas porosity or shrinkage porosity. The pressure is several orders of magnitude greater than the melt pressures developed in conventional foundry practice. Consequently, melt feed from hot spots into incipient shrinkage pores is achieved much more readily. The high applied pressure also keeps entrapped gases in the solution and promotes intimate contact between casting and tooling for rapid heat extraction and fine resulting microstructure. Additionally, squeeze casting requires no runners and gates and parts can be made to near net shape with a minimum amount of materials and energy utilization [11].

The concept of squeeze casting is believed to have originated in Russia nearly a hundred years ago. But the process has recently been into commercial use in Europe and Japan to produce high quality engineering components with and without fiber reinforcement [15].

Both casting and forging have well known inherent advantages for producing metal parts in volume. Sand casting usually starts with a low cost molten metal and in one operation produces extremely

complex shapes. Forging, starts with a preform of a wrought material and produces shapes that are less complex but have closer dimensional accuracy, smoother surfaces and higher mechanical properties. On the minus side, conventional forgings usually require several sets of dies to transform a bar or other preform shape into a ready-to-machine part. Furthermore, a wrought preform is more expensive than one that has been cast. Castings also have lower strength and rougher surfaces than forging. The need to combine the advantages and eliminate the disadvantages of these techniques has led to the development of the squeeze casting technique [16].

Squeeze casting sequence has four main steps [11], as seen in Fig.2.1 : a) Melting the material; preheating the the tooling, lubricating the tooling, b) Transferring the melt into the die cavity, c) Applying the pressure until complete solidification is reached, d) Ejecting the casting, cleaning the tooling and recharging the furnace.

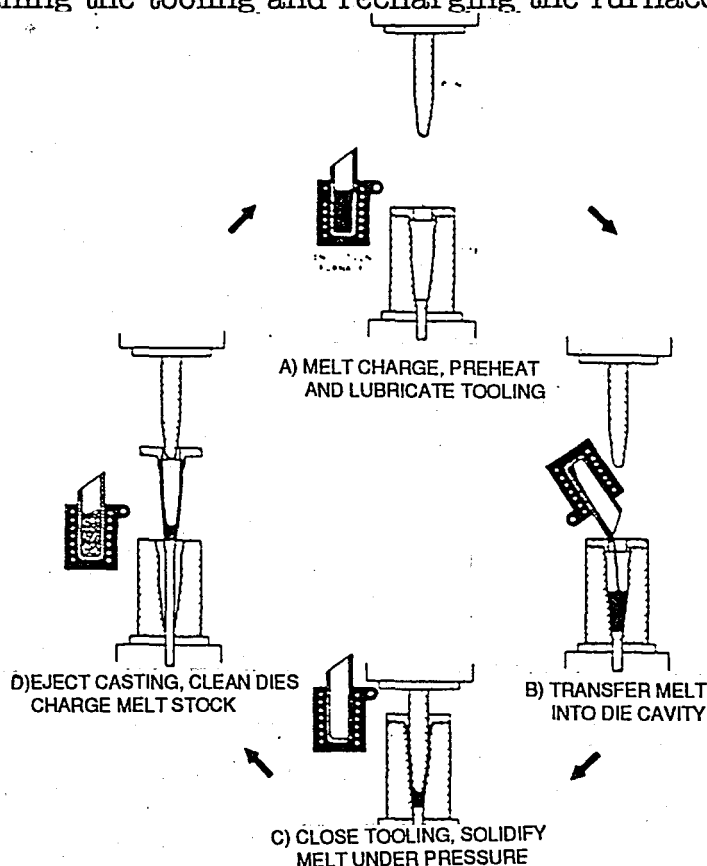


Fig. 2.1. Tooling and processing sequence for squeeze casting [11].

In general, two different methods of squeeze casting are available based upon different approaches to metal metering and movement: 'direct' and 'indirect' squeeze casting methods [15]. In the direct squeeze casting method the pressure is applied to the entire surface of the liquid metal during freezing. This method provides the most rapid heat transfer, yielding the finest grain structure. Although flat-topped ingots can be produced by means of direct squeeze casting method, more complex castings to finished shapes can be produced by means of a shaped punch [15], (Fig. 2.2). As an example, Fig. 2.3 illustrates the process for the squeeze forming of a vehicle wheel. A metered volume of metal is poured into the lower die set, after which an upper punch is lowered to displace the metal in the closed die. High pressure is then applied to ensure a high integrity part for high performance. The cycle is divided into seven discrete stages as itemized in Table 1 [17].

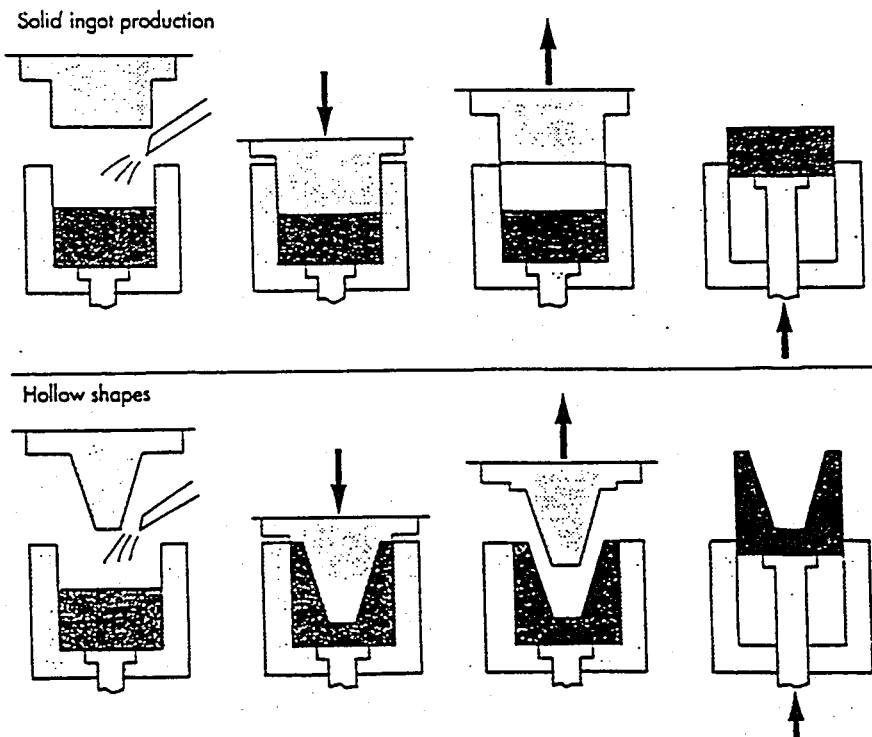


Fig. 2.2. Production of solid ingot and hollow shapes by 'direct' squeeze casting process [15].

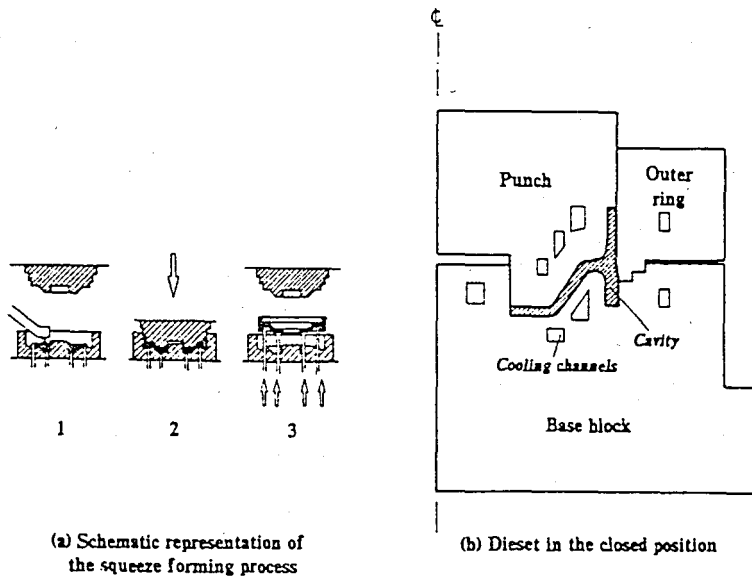


Fig. 2.3. The squeeze forming process and associated tooling design for the production of a vehicle wheel [17].

Table 2.1. Stages in the squeeze forming process of the vehicle wheel given in Fig. 2.3 [17].

Stage	Time (sec)
1. Die surface coating application	8-10
2. Die filling	18
3. Punch approach to the metal surface	10
4. Die closure and metal extrusion	5-35
5. Pressure buildup	2-65
6. Pressurized solidification	57
7. Die opening and part ejection	16

In the indirect squeeze casting process, metal is injected into the die cavity by a small diameter piston, by which mechanism the pressure is also applied during freezing (Fig. 2.4). This technique is really a hybrid process between pressure die casting and squeeze casting, and the cast product is not of the superior quality as is obtained from the direct squeeze casting process. Another disadvantage of this method is that the material utilization is often inefficient in that a runner and gating system is used and this material has to be removed and recycled. Of the two methods for squeeze casting it appears that the direct process is more common in practice for the production of full integrity castings and metal matrix composites.

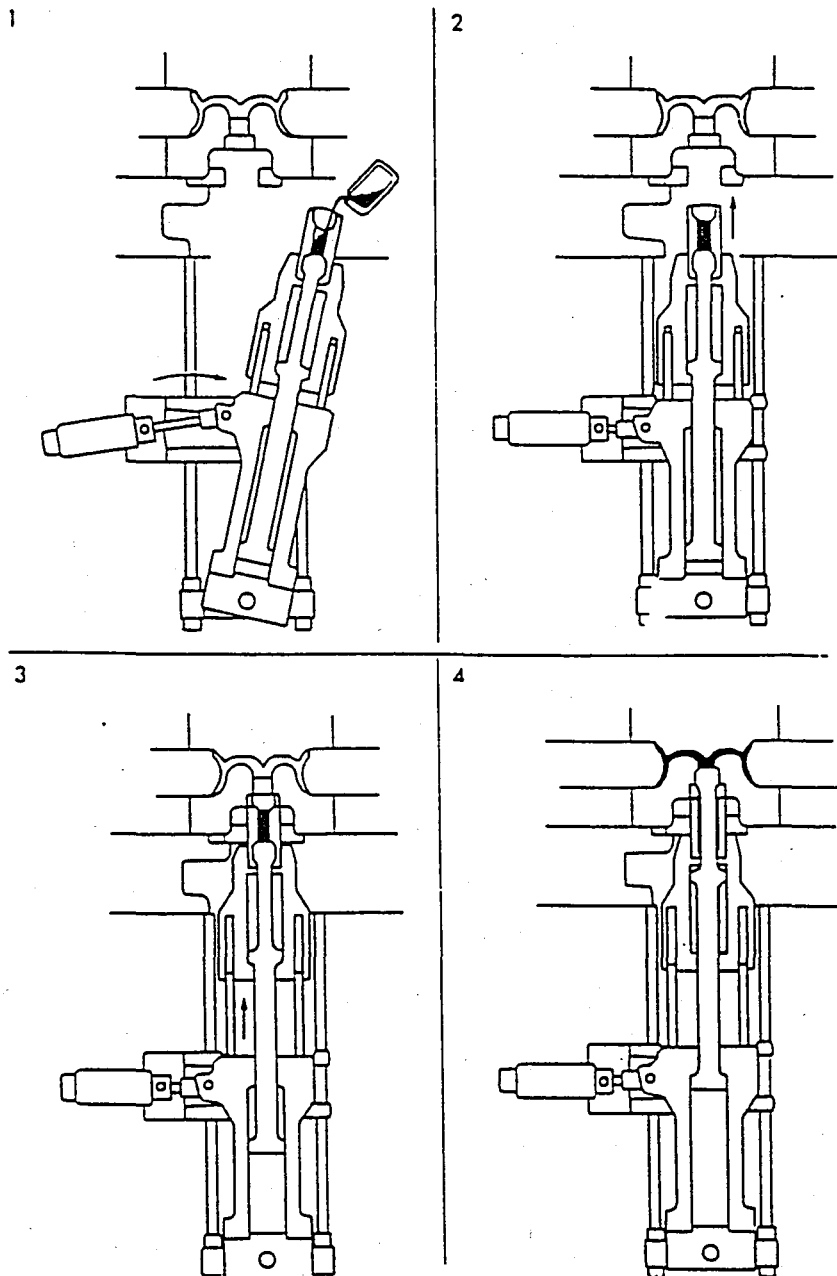


Fig. 2.4. Ube vertical shot indirect squeeze casting system: 1. pouring aluminum, 2. injection cylinder swivels to original position, 3. sleeve holder goes up with sleeve and sets in bottom die, 4. plunger tip goes up and injects [15].

The factors that influence the quality of the product in the squeeze casting method are listed below in decreasing order of importance: Melt quality and quantity, equipment and tooling, casting temperature, tooling temperature, time delay before pressure application, lubricant film thickness and its adherence, and pressure level and duration [11]. Although the pressure is the main factor it is listed at the bottom of the list because it is usually provided more than the required level in practice.

2.1.1. Melt Quality and Quantity

Melt quality especially in terms of oxide content is perhaps more critical in squeeze casting than in gated processes. Because in squeeze casting there are no runners and gates to accommodate any dross that may be present. All of the melt that poured into the die generally stays in the casting. But on the other hand, melt quality in terms of absorbed gases is less critical in squeeze casting than in other methods, because the pressure level is selected to be high enough to suppress gas evolution and to retain gases in solution. For both ferrous and nonferrous alloys the oxide content must be minimized whenever possible by a combination of fluxing, skimming and/or filtering. But, since the gas porosity is overcome by pressurization the degassing treatments are unnecessary.

The quantity of the casting is important for the dimensional accuracy of the casting. Since the dies are originally held in the open position, they do not define a closed cavity with a definite volume. Thus, a method is needed to meter the proper amount of molten metal into the die cavity. One approach is to design the die system so that any excess metal is pushed out of the die cavity prior to application of pressure and to be trimmed subsequently. A second method is to control the level of the melt in the ladle or furnace, and design the

squeeze casting dies so that any excess metal causes variation only in noncritical dimensions. A third type of metering system would feed the exact amount of molten metal into the die cavity. Such systems are available for metering cast irons in large quantities, especially for large diameter lightweight parts but, for metering small quantities it is very difficult to obtain any degree of accuracy [16].

2.1.2. Equipment and Tooling

Hardware requirements for squeeze casting are relatively simple unless reentrant profiles are to be cast to net shape. Even then the tooling for squeeze casting is simpler in construction than those used in forging, die casting or permanent mold casting. As seen in Fig. 2.1 the main elements of the tooling are a punch, a die and a knock-out pin to eject the casting. The tooling is mounted for use in a hydraulic press which may be single action or double action, depending on the part geometry and pressure requirements [11].

The die material for squeeze casting is usually H13 grade Cr-Mo hot work die steel. This material combines moderate high temperature strength with adequate resistance to wear and thermal fatigue. For ferrous applications the portions where the molten steel contacts are usually made of tungsten base and molybdenum base materials (e.g., Anviloy 1150) for other parts H13 hot work die steel is used [13].

In squeeze casting the shape and the size of the component have an important influence on die life. Massive die sections and those do not have small projecting portions that become enveloped by the molten metal are seldom damaged from plastic deformation or heat checking. On the other hand the parts that form narrow deep details in the casting may require periodic replacement. Die design is also very important for die life and for pressuration level.

In Fig. 2.5 two different die designs for the same shape are illustrated. The results of the elongation and tensile strength tests of various section thicknesses of the both components are shown in Fig. 2.6. By comparing the results an increase in mechanical properties is noted for design A; a backward filling system. In design A the poured melt is first cooled at the bottom of the die cavity and then pushed up into the thin section by pressure. But in design B, the melt is directly poured into the thin section and solidified before pressure application [12].

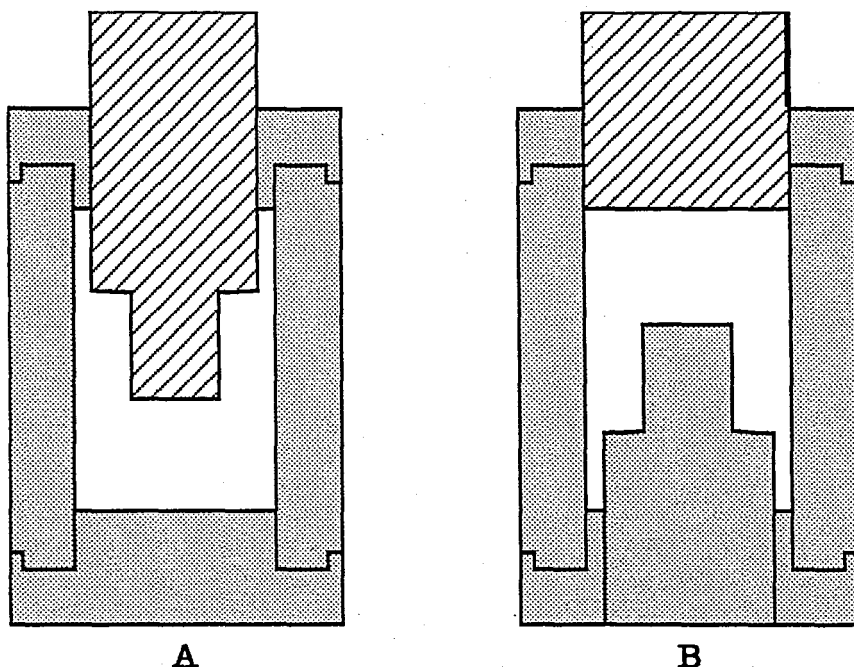


Fig. 2.5. Two different squeeze casting die designs for the same shape [12].

It is generally preferred to design the tooling to provide directional solidification of the squeeze casting in a direction such that the semi-liquid regions of the casting continue to experience punch pressure. When it is not practical to accomplish this as is frequently the case with irregular shapes, a higher level of pressure is found to be required to consolidate the casting.

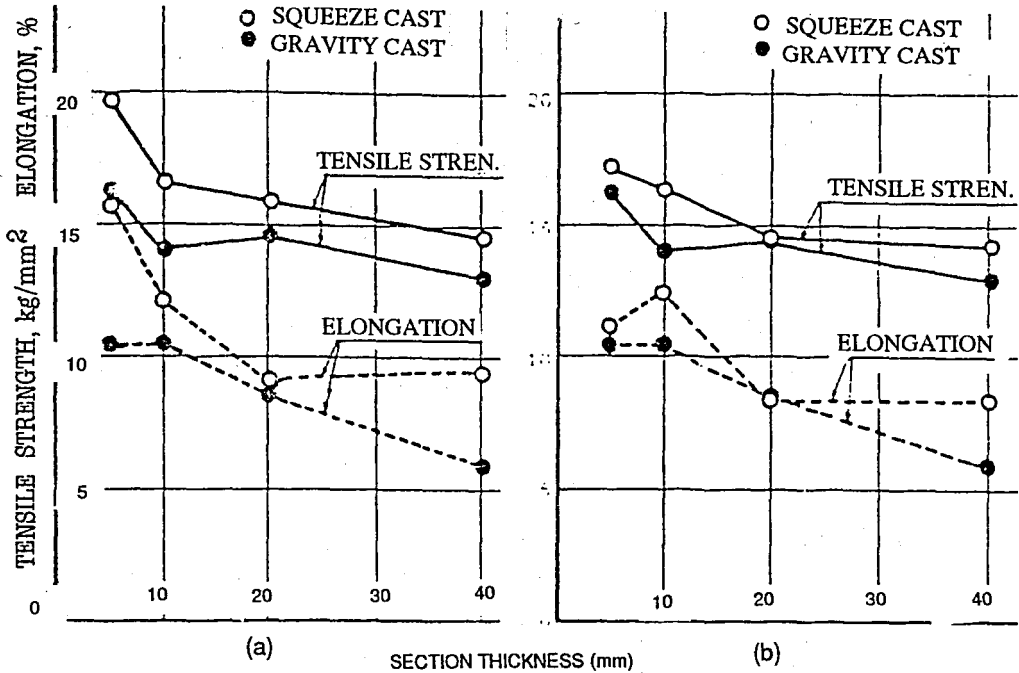


Fig. 2.6. Relation between mechanical properties and section thickness; (a) for design A, (b) for design B [12].

2.1.3. Casting Temperature

The temperature at which the molten metal is poured into the die cavity is extremely critical from the standpoints of both casting quality and die life. Too low a casting temperature causes inadequate fluidity in the melt during die filling and results in incomplete die fill as well as cold laps on the casting surfaces. But, on the other hand if, the casting temperature is too high this can cause extrusion of liquid metal through the tooling interfaces and can also result in shrinkage porosity in thick sections of the casting. And the die life is adversely affected by high pouring temperatures.

The ideal pouring temperature depends both on the liquidus temperature, T_L , and the freezing range, ΔT , (the difference between liquidus (T_L) and solidus (T_S) temperatures) of the alloy. In general alloys having a narrow freezing range requires more superheat.

Castings with thin sections and nonuniform profiles also require a higher casting temperature to promote die filling. This superheating level changes between 10 °C to 100 °C for aluminum alloys and 30 °C to 150 °C for Cu-base alloys and steels [11].

2.1.4. Tooling Temperature

In squeeze casting the temperatures of the die cavity and the punch are usually maintained between 200 °C and 300 °C. Low temperatures (lower than 150 °C) may cause thermal fatigue failures in the dies and also cold laps on the surfaces of the casting. On the other hand, very high tooling temperatures (higher than 400 °C) can cause hot spots and shrinkage pores in the casting. Another problem with overheated dies (especially for ferrous applications) is the tendency for welding between the casting and the die [11].

2.1.5. Time Delay Before Pressure Application

In the squeeze casting processes optimum results are obtained when the pressure is applied near the zero fluidity temperature of the molten metal. Where the zero fluidity temperature is defined as the temperature below which the metal loses its fluid flow properties. It is usually midway between the solidus and liquidus temperatures of the alloy. But as it is not practical to pour the melt into the die at or below its liquidus temperature, the melt is usually poured superheated and pressurized after allowing it to cool below liquidus temperature.

2.1.6. Lubrication

Normal parting agents are not applicable in squeeze casting because of their limited adherence to the tooling under pressurized transverse flow of semi-liquid metal. A thin layer of colloidal graphite sprayed on

the hot dies before pouring is usually satisfactory for non-ferrous and cast iron applications. But for steel castings the die surfaces which make contact with the molten steel must be sprayed with a ceramic parting agent when they are hot. For all applications it is desirable to pretreat the dies by heating them in air to 350 °C, thereby depositing a protective oxide coating to inhibit galling and welding. Coating or mold-washing the surfaces in contact with the molten metal with graphite or with a ceramic parting agent also enhance the casting surface finish.

2.1.7. Pressure Level and Duration

Usually the pressure level for most ferrous and non-ferrous squeeze castings is 70-105 MPa in order to eliminate shrinkage and gas porosity. However, it is the geometry of the casting that generally dictates the use of higher pressures for die filling and porosity control. There is a critical pressure for each composition at which density nearly reaches saturation. The saturation values are almost equal to the ideal (theoretical) density of the alloy of that composition. This pressure level is called as "the critical pressure for density". There is also a critical pressure above which no defects (porosity, shrinkage etc.) are detected (by dye penetrant checking) and this pressure is called as "the critical pressure for defects". Usually the critical pressure for defects is higher than the critical pressure for density and it dictates "the minimum pressure level" for a sound casting [12].

For example, in the investigation of response of three cast aluminum alloys to squeeze casting it is found that each aluminum alloy was characterized by a critical minimum pressure required for radiographic soundness, and that the threshold pressure was dictated by the freezing range of the particular alloy [11]. In general, a pressure of 105 MPa was necessary to eliminate porosity in alloys

with a narrow freezing range ($\Delta T \approx 10$ °C), where as 70 MPa was adequate for alloys with extended freezing range ($\Delta T \approx 100$ °C). Extended freezing range alloys were found to require less applied pressure because of shorter feed length between the semi-liquid pool and solidifying metal than for narrow freezing range alloys [11].

When the casting is thin or non-uniform in cross section there is frequently a portion of the casting which solidifies first and thereafter takes the bulk of the applied load. This prevents hydrostatic transmission of pressure to 'burst feed' hot melt into incipient pores. To eliminate porosity in such cases, the applied load should be such that it plastically deforms the solidified crust and has enough pressure left for the remainder of the casting.

Raising the pressure level above the the minimum pressure level consistent with sound castings has been found to provide little additional benefit, although extremely high pressures exceeding the yield stress of the casting have been reported to provide grain refinement and higher properties. But, this added benefit must be weighed against the increased costs resulting from a higher press capacity requirement and the reduced die life due to combination of high pressure and temperature [11].

The pressure level in squeeze casting is usually in the range of 70-105 MPa for simple shapes and rises to 140-210 MPa for thin sections and complex shapes. The shape and the section thickness of the casting governs the duration of pressure necessary to ensure complete solidification under pressure. And the approximate duration of pressure can be calculated as 1 sec per mm of section thickness [11].

2.2 Application of Squeeze Casting in Metal-Matrix Composites

Squeeze casting has become one of the accepted liquid metal routes for efficient and effective production of metal-matrix composites (MMC's) using ceramic preforms or particles. In Table 2.2, it is understood that the squeeze casting route in fact is already accepted as the standard method in producing commercial MMC production [7]. This acceptance is based on the fact that squeeze casting produces "zero porosity" composites. The theoretical value of the pressure needed for the infiltration of liquid metal through fiber preform depends on the system, i.e., whether it is 'wetting' or 'non-wetting'. Fig. 2.7 shows schematically the movement of liquid metal front through an idealized parallel bundle of fibers in which the equilibrium wetting angle is assumed to be a characteristic physical property of the system (the influence of metal movement on the magnitude of wetting angle is neglected). In general a low wetting angle between the phases will aid infiltration but too low a wetting angle might create such effective load transfer so as to endow the composite with a low fracture toughness. Too high a wetting angle will increase the difficulty of preform infiltration especially for dense preforms, and residual porosity in the MMC's will be more probable. So, for optimizing the load transfer and toughness, much effort is being expended on finding more suitable surface coatings for fibers [18].

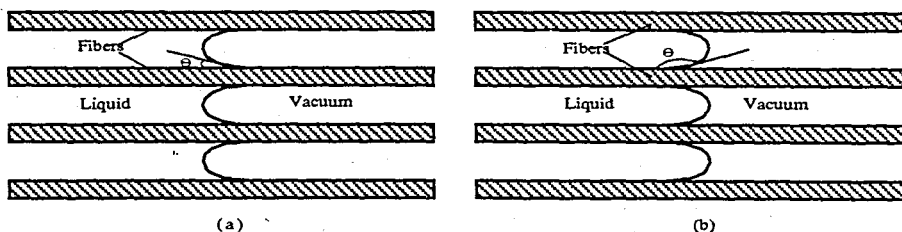


Fig. 2.7. Movement of liquid metal through parallel fiber bundles (a) wetting system, (b) non-wetting system [18].

Table 2.2. The practical application of cast MMC's for commercial products in Japan [7].

Product	MMC system	Method of manufacture	Characteristics of applied MMC	Year (maker)
Ring groove reinforced piston	Al ₂ O ₃ /Al alloy	Squeeze casting (SC)	Light weight, wear resistance at high temperature	1983 (Toyota)
Golf goods Face of screwdriver	SiC _p /Al alloy	SC	Light weight, abrasion resistance	1984 (Nippon Carbon)
Connection rod of gasoline engine	SUS fibre/Al alloy	SC	Specific strength	1985 (Honda)
M6~8 bolt	SiC _w /6061	SC, extrusion, tread rolling	Neutron absorption, high temperature strength, little degassing	1986 (Toshiba)
Vane, pressure side plate of oil pressure vane pump	Al ₂ O ₃ .SiO ₂ /AC4C	SC	Wear resistance, noise damping	1987 (Hiroshima Aluminium)
Joint of aerospace structure	SiC _w /7075	SC, rolling	Specific strength, low thermal expansion	1988 (Mitsubishi Electronics)
Rotary compressor ane	SiC _w /Al-17% Si-4% Cu alloy	SC	Specific strength, wear resistance, low thermal expansion	1989 (Sanyo)
Shock absorber cylinder	SiC _p /Al alloy	Compcasting, SC, extrusion	Light weight, wear resistance, thermal diffusion	1989 (Mitsubishi Aluminium)
Diesel engine piston	SiC _w /Al alloy	SC	Light weight, wear resistance	1989 (Niigata)
Cylinder liner	Al ₂ O ₃ , CF/Al alloy	Low pressure SC	Light weight, wear resistance	1991 (Honda)
Hub of damper pulley ¹⁰	Al ₂ O ₃ .SiO ₂ /Al alloy	SC	Light weight, reduction of vibration	1991 (Toyota)

The theoretical total pressure differential, ΔP , required to infiltrate a preform is dependent on four separate terms [18]:

$$\Delta P = P_o - P_g = \Delta P_\gamma + \Delta P_\eta \quad (2.1)$$

Where P_o is the pressure on the liquid metal at the surface of the preform, P_g is the gas pressure within the preform, ΔP is the Gibbs-Thomson pressure at the liquid front and ΔP_η is the pressure drop owing to flow through the porous preform. The infiltration of a preform therefore depends on the wetting angle, the preform density and geometry, the back pressure in the preform and the applied pressure [18].

There is a particular pressure differential due to capillary forces at the liquid metal front during infiltration of the reinforcement. It is this pressure differential that determines whether infiltration will be spontaneous (wetting systems) or will require applying pressure to the liquid metal (non-wetting systems). In the case of a non-wetting system, the squeeze casting method is a suitable way to supply pressure to the system. The pressure differential at the liquid/metal front is given by the Young-Kelvin equation [19]:

$$P = \sigma_{LA} \cdot \kappa \cdot \cos \Theta \quad (2.2)$$

Where σ_{LA} is the liquid metal/atmosphere interfacial energy, κ is the curvature at that interface and Θ is the contact angle. The energy W given off process per unit volume is;

$$-W = (\sigma_{FL} - \sigma_{FA}) \cdot S_f \quad (2.3)$$

Where S_f is the fiber surface area per unit volume of metal matrix, σ_{FL} and σ_{FA} are the interfacial energies of fiber/liquid metal and fiber/atmosphere respectively. Now since,

$$W = -P \cdot \Delta V \quad (2.4)$$

Where ΔV is the volume over which the metal was displaced, for a unit volume of metal matrix ($\Delta V=1$) one can obtain,

$$P = (\sigma_{FL} - \sigma_{FA}) \cdot S_f \quad (2.5)$$

In particular, for a bundle of fibers of diameter d_f , occupying a volume fraction V_f :

$$S_f = \frac{4 \cdot V_f}{d_f \cdot (1-V_f)} \quad (2.6)$$

for fiber bundles and,

$$S_f = \frac{6 \cdot V_f}{d_f \cdot (1 - V_f)} \quad (2.7)$$

for spherical particles and, the final expression for fiber bundles becomes,

$$S_f = \frac{4 \cdot V_f \cdot (\sigma_{FL} - \sigma_{FA})}{d_f \cdot (1 - V_f)} \quad (2.8)$$

and,

$$S_f = \frac{6 \cdot V_f \cdot (\sigma_{FL} - \sigma_{FA})}{d_f \cdot (1 - V_f)} \quad (2.9)$$

for spherical particles.

If σ_{LA} is known the term $(\sigma_{FL} - \sigma_{FA})$ can be calculated from the work of adhesion,

$$W_a = \sigma_{LA} + \sigma_{FA} - \sigma_{FL} \quad (2.10)$$

or, from the contact angle when it is finite (imperfectly wetting or non-wetting systems), since

$$\sigma_{FA} - \sigma_{FL} = \sigma_{LA} \cdot \cos \theta \quad (2.11)$$

For nonsmooth fiber or particle surfaces an adequate factor $f > 1$ may be needed as a multiplier of S_f .

The instantaneous pressure differential will actually vary during infiltration. For wetting systems S_f will decrease and P which is

negative will will increase with time. And in non-wetting systems S_f will increase with time and P which is positive will increase with time. In some theoretical cases P goes to infinity. Now, consider a simple two dimensional wedge, of half angle α at its base as seen in Fig. 2.8(a). It is assumed that the metal does not wet the fiber material with,

$$(\sigma_{FL} - \sigma_{LA}) < \sigma_{FA} < \sigma_{FL} \quad (2.12)$$

The infiltration pressure given from the thermodynamic principles for that geometry is [19],

$$P = \frac{\sigma_{LA} \cdot \sin(\theta - \alpha - \pi/2)}{L \cdot \sin \alpha} \quad (2.13)$$

As we notice from Eq. 2.13, P is positive and goes to infinity as L goes to zero. Now consider the contact point of two equal fibers or spherical particles in Fig. 2.8(b). For cylindrical particles we obtain:

$$P = \frac{\sigma_{LA} \cdot \sin(\theta - \alpha - \pi/2)}{R \cdot \sin \alpha \cdot \text{Tg}(\alpha/2)} \quad (2.14)$$

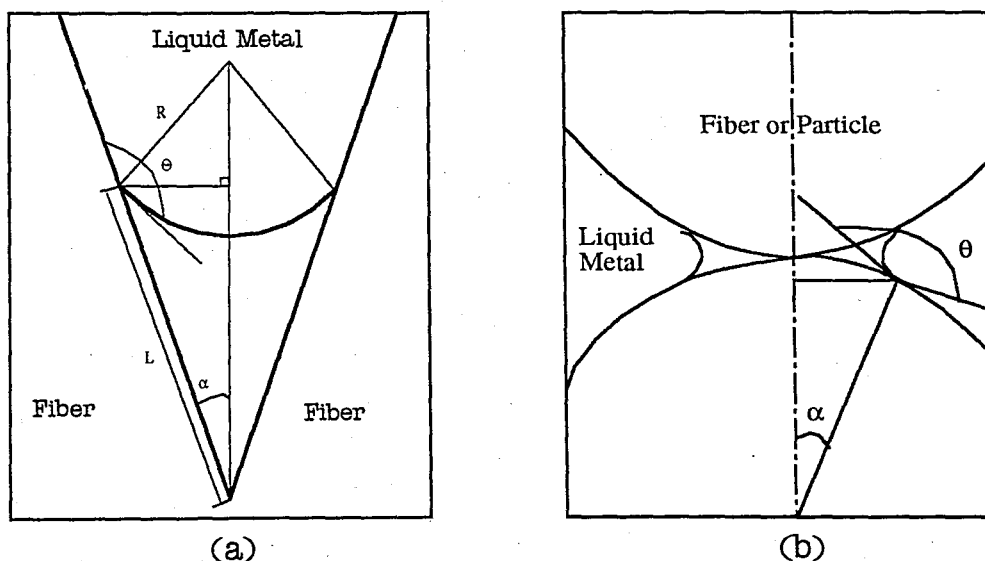


Fig. 2.8. Infiltration of (a) a wedge, (b) the contact area between two fibers or spherical particles by a non-wetting metal [19].

and,

$$P = \frac{\sigma_{LA}}{R \cdot \sin \alpha} \left[\frac{\sin(\Theta - \alpha - \pi/2)}{\text{Tg}(\alpha/2)} - 1 \right] \quad (2.15)$$

for spherical particles.

In both cases the pressure for infiltration becomes infinitely large when α approaches to zero [19]. These pressures are usually in between 100-200 MPa for most common MMC systems. Hence, we can say that squeeze casting is a very suitable way for MMC production [7-10].

In Fig. 2.9 the variations of melt and die temperatures versus time for monolithic A357, manufactured by gravity die casting and squeeze casting at 100 MPa are shown. When the pressure is applied at the eutectic temperature of the melt an abrupt decrease in temperature occurs at both the center and the edge of the ingot. The application of pressure causes intimate contact between the molten metal and the die surface, allowing heat to be extracted by an order of magnitude faster than the gravity die casting. High pressure also increases the undercooling in the melt, with a corresponding increase in the number of nucleation sites [8].

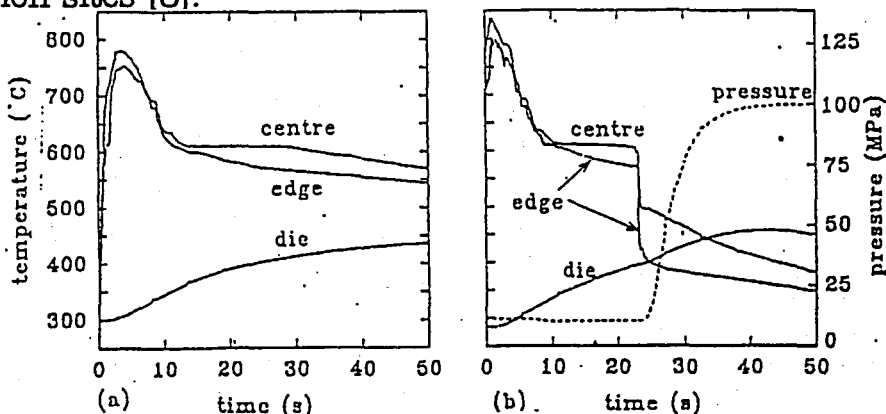


Fig. 2.9. Melt and die temperatures versus time for monolithic A357 during (a) gravity die casting and (b) squeeze casting at 100 MPa [8].

It is also reported that [8] the resulting microstructure in squeeze casting is the same as in gravity die casting but, the increased rate of heat extraction and corresponding increased undercooling and solidification rate led to (1) refinement of the dendrite structure; (2) an increase in volume fraction of Al dendrites and (3) a decrease in volume fraction of eutectic.

The same type of structures are observed for the matrix of A357/Steel MMC and also rapid solidification due to applied pressure resulted good contact between matrix and preform insert. Also in A357/A356/SiCp MMC's and in A357/Al₂O₃ short fiber MMC's squeeze casting is reported as a suitable way for locally reinforced MMC's by Kang et al [8]. Also Fukunaga et al [9, 10] reported that when the squeeze casting method is applied in devitroc ceramic fiber reinforced aluminum to produce general purpose machine parts, it improved the tensile strength at elevated temperatures, wear resistance and damping characteristics of these materials.

2.3. Comparison of Squeeze Casting Method With Other Methods

As mentioned at the beginning, squeeze casting is an hybrid process developed to combine the advantages and to eliminate the disadvantages of metal forming methods. With optimized parameters, squeeze casting allows significant improvements in mechanical properties of the materials. For example, in Fig. 2.10 comparison of mechanical properties of a magnesium alloy AZ91 are sketched as a function of casting method. In Tables 2.3 and 2.4 comparative properties of commercial ferrous alloys and JIS AC4ET6 (356-T6) aluminum alloy castings are shown.

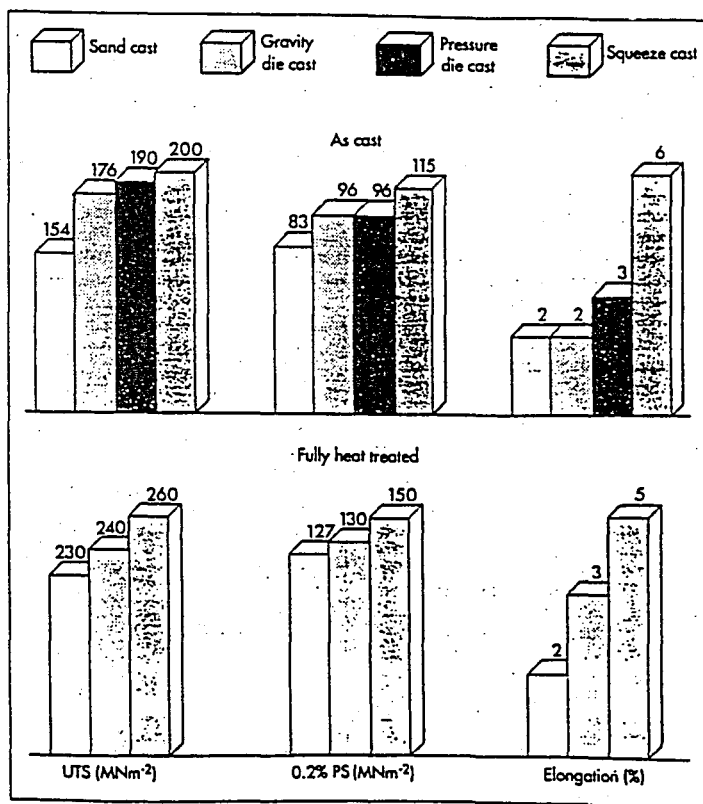


Fig. 2.10. Mechanical properties of squeeze cast and fully heat treated AZ91 as a function of casting process [15].

Table 2.3, Comparative properties of commercial ferrous alloys [11].

Alloy	Process	Tensile Strength.		Yield Strength.		Elongation Pct
		MPa	ksi	MPa	ksi	
347 S.S. (Annealed)	Squeeze casting ¹	614	89.0	303	44.0	46
	Sand casting	400	58.0	241	35.0	20
	Extrusion	621	90.0	241	35.0	50
321 S S (Heat Treated)	Squeeze casting ²	1063	154.2	889	129.0	15
	Forging ²	1077	156.2	783	113.6	7
Fe-0.25 pct C-0.75 pct Mn -0.50 pct Si-0.50 pct Ni- 0.55 pct Cr, 0.55 pct Mo	Squeeze casting ¹⁷	952	138.0	903	131.0	14
	Sand casting ¹⁷	1131	164.0	1038	150.5	10

Table 2.4. Comparative properties of JIS AC4C-T6 (356-T6) aluminum alloy castings [11].

Process	Tensile Strength		Elongation Pct	Hardness HV(5 kg)	Charpy Impact Value		Fatigue Strength (10^7 cycles)	
	MPa	ksi			J/mm ²	ft-lb/in ²	MPa	ksi
Squ. casting	295	42.8	12.5	105	0.18	86	124	18.0
Gra. casting	280	40.6	2.4	103	0.03	14	85	12.3

El Mahallawy et al [20] applied squeeze casting method to the Al-7%Si alloy and found the volume fraction of macroporosity in squeeze cast samples as 0.1%, while it was 4.0% in gravity cast samples. And, the amount of microporosity decreased from 2% to 0.003% for a specimen obtained by squeezing under 68.67 MPa. Also the mechanical properties increased with the applied squeezing pressure in the same study. In Figs. 2.11 and 2.12 the changes in tensile strength, fracture strain and impact toughness of Al-7%Si alloy with increasing squeezing pressure are shown.

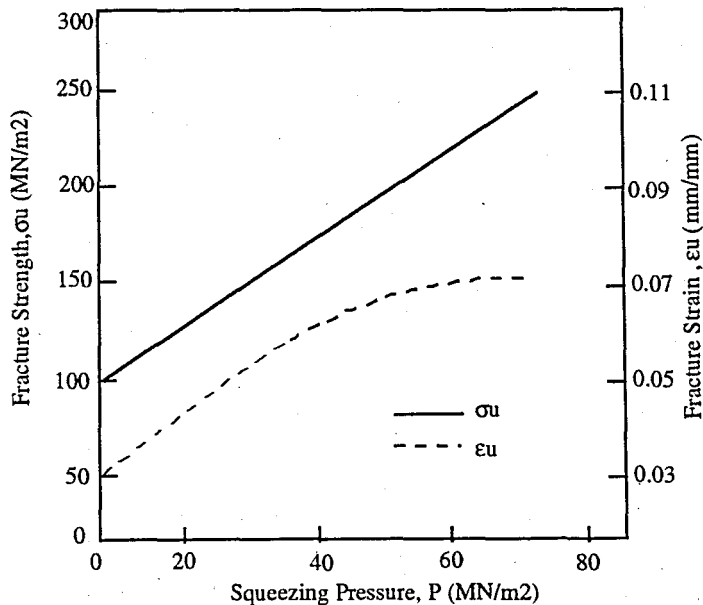


Fig. 2.11. Variation of fracture tensile strength and fracture strain with squeezing pressure in Al - 7%Si alloy [20].

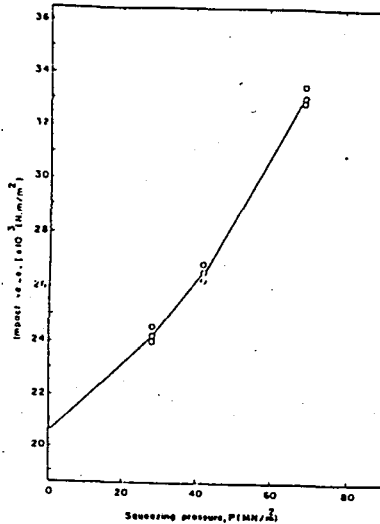


Fig. 2.12.. Variation of impact toughness with squeezing pressure in Al -7%Si alloy [20].

Squeeze casting not only eliminates porosity and refines microstructure of the casting but also permits the use of alloys traditionally difficult to cast but which offer high fatigue strength. Even for a conventional alloy the gain in fatigue strength can be significant. In Fig. 2.13 the fatigue curves of pistons made of E-332-T5 aluminum are plotted. The microstructural refinement in squeeze casting over permanent mold casting as evidenced by the fatigue strengths appears to hold up even during elevated temperature testing (200 °C) to simulate engine service [11].

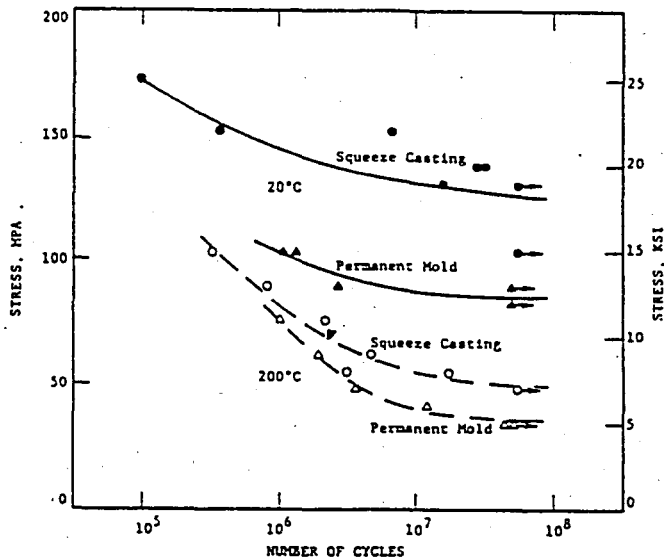


Fig. 2.13. Fatigue curves for diesel engine pistons (E332-T5 Al) produced by squeeze casting and gravity die casting [11].

Kaneko et al [11] rated casting methods for a variety of automotive applications based on economy, product reliability, design flexibility and part complexity (Fig. 2.14). As can be seen from this figure and other results, squeeze casting can be rated as an ideal manufacturing process with respect to the other methods.

	Gravity Casting	Die Casting	Forging	Squeeze Casting
Economy	C	A	D	B
Reliability	C	D	A	B
Design Flexibility	A	C	D	B
Complexity	C	A	D	B

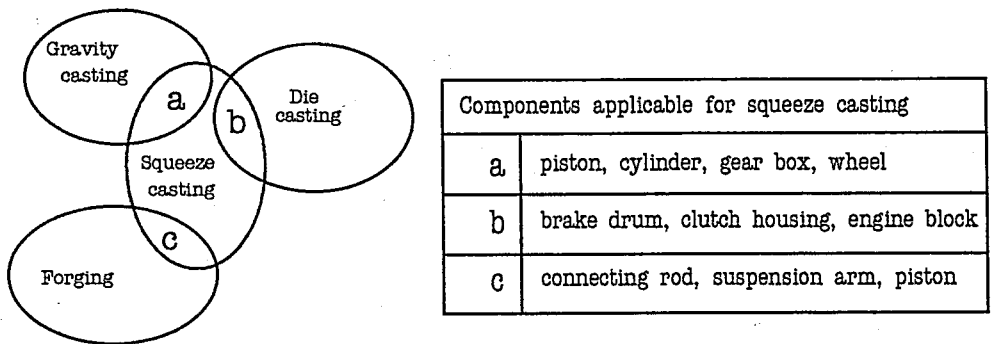


Fig. 2.14. Squeeze casting rating and potential automotive applications [11].

The major advantages of squeeze casting over the other casting processes are as follows [11-15]:

a) Materials having neither gas porosity nor shrinkage porosity are produced.

b) No feeders or risers are required and therefore no metal wastage occurs.

c) The inherent castability of the alloy is of little or no concern since the applied pressure deviate the need for customary high fluidity. Both common casting alloys and ostensibly wrought alloys can be squeeze cast to finished shape.

d) Control of microstructure is possible solely by control of the dominant process parameters such as pouring temperature and mold temperature. Nucleating agents can be used but, they are not normally necessary.

e) Because there are no internal and external defects on a properly produced squeeze cast component costly post solidification examination by non-destructive testing techniques is of very limited value.

f) Squeeze castings can have mechanical properties as good as , and in some cases even better than wrought products of the same composition. Their casting factor should therefore, be set at unity.

g) Squeeze casting provides the most effective and efficient route to produce nearly net-shape composite components for engineering applications. It produces complex shapes and fine details beyond the scope of forging.

h) Squeeze casting requires less pressure than hot or cold forging, reducing equipment and die material requirements. Together with the use of a lower cost starting material (melt stock), these factors make squeeze casting considerably less expensive than forging.

i) Squeeze casting process also allows fiber preforms to be placed in critical areas of the component where high performance is required or it can be used in the production of MMC's with ceramic fiber preforms.

j) Labor associated with sand casting such as for molding, trimming of risers and gates and cleaning of casting is eliminated.

k) It increases the production rates in comparison with conventional casting techniques.

In realizing these benefits, there are several factors to be considered and problems to be solved for squeeze casting applications. So, the disadvantages of squeeze casting for today can be listed as:

a) The oxide level of the melt is more critical than it is in gated casting processes. Therefore it must be minimized if, possible.

b) The process needs a close control of tooling temperature and a

good timing for pressure application. Because these parameters highly effect the quality of the casting.

c) Squeeze casting is very hard to apply for the narrow freezing range alloys, because of their needs for high overheating temperatures resulting extrusion of liquid metal through tooling interfaces and shrinkage porosity in thick sections.

d) Lubrication is very important in order to prevent contact welding resulting from the high pressure and die temperature and to provide good surface finish.

e) Squeeze casting method is not suitable for extremely complex shapes or parts with a very narrow cross section.

2.4. MONOTECTIC SOLIDIFICATION

2.4.1. Monotectic Phase Diagram

The monotectic reaction is very similar to the eutectic reaction except that one of the product phases is a second liquid phase. In eutectic reaction the liquid (L) decomposes into two solid phases S_1 and S_2 at a composition of C_e and temperature T_e according to the reaction $L \Rightarrow S_1 + S_2$. But in monotectic reaction the liquid L_1 decomposes into a solid phase S_1 and another liquid phase L_2 at a monotectic composition C_m and temperature T_m according to the reaction $L_1 \Rightarrow S_1 + L_2$.

The monotectic phase diagram is characterized by a dome-shaped region, where two immiscible liquid phases exist. In Fig. 2.15 a typical monotectic phase diagram is shown. The homogenous liquid L_1 , having a monotectic composition transforms to the solid A and B-rich liquid L_2 simultaneously through the monotectic reaction at a constant monotectic temperature. The monotectic alloys have such proprietary

characteristics that both A and B elements are almost insoluble in each other in the solid state, liquids L_1 and L_2 have very different densities and the alloy has a liquid miscibility gap which is very wide. So, in hypermonotectic alloys it is never easy to obtain a homogenous melt, and alloys having compositions within the liquid miscibility range solidify, accompanied by heavy gravity segregation before the monotectic reaction begins. These problems have delayed the utilization of monotectic alloys as industrial materials [2]. To overcome these problems, experiments are being carried on in space (microgravity), in cyclic gravity environment and during parabolic flight [3-6].

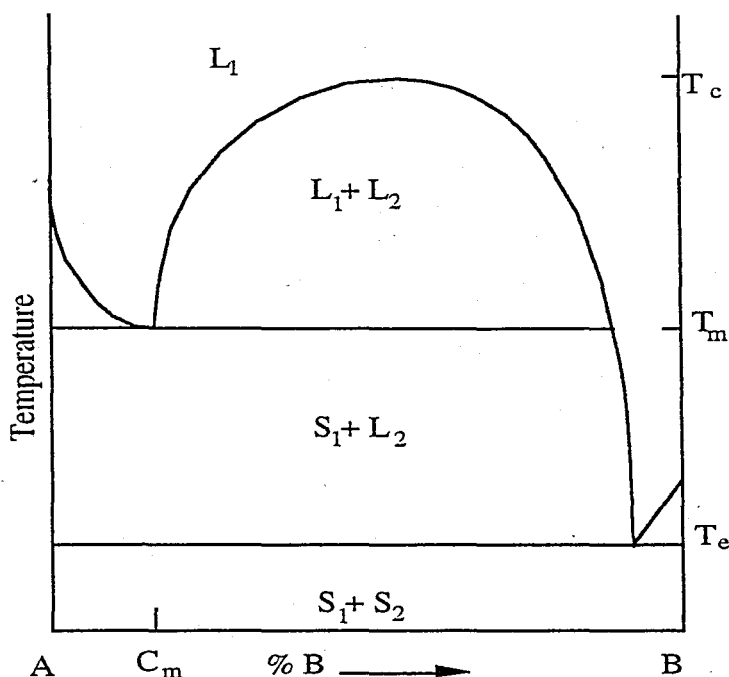


Fig. 2.15. Typical monotectic equilibrium diagram [22].

In monotectic reaction the ratio of the two product phases is given by the application of the lever to the monotectic horizontal; it appears that in all known monotectic systems the amount of the solid phase produced is always greater than the amount of the liquid phase produced [22]. This means that in monotectic systems the solid phase forms a continuous matrix, whereas the liquid phase is discontinuous, being retained in isolated pockets within the solid matrix.

2.4.2. Normal (Bulk) Monotectic Freezing

Above the monotectic temperature T_m , the alloy of composition M is a homogenous liquid (L_1) as seen in Fig. 2.15. At or slightly below T_m , the alloy enters the two phase field of (S_1) and (L_2), and when these phases have once nucleated, a total of three phases are then present in the alloy. Since the Gibb's phase rule states that in a system containing (C) components and (P) phases in equilibrium the number of degrees of freedom (F) is given by the relation;

$$P+F=C+1$$

The phase rule then specifies that under these circumstances (i.e. two components, three phases) the system has zero degrees of freedom ($F=0$). The temperature therefore remains constant until the liquid L_1 has decomposed completely to solid α and liquid L_2 . The decomposition of L_1 takes place by the growth of large dendritic crystals of α -phase into the liquid, which becomes supersaturated with respect to L_2 due to the rejection of component B from the solid α . If the liquid L_2 nucleates in the vicinity of the solid α -phase and if L_2 were to completely surround the solid phase, the growth of these α -crystals could be stifled in much the same way as in peritectic freezing. However, everything depends upon the density of L_2 relative to L_1 and also whether L_2 wets α -phase dendrites or not [22].

If the new liquid phase L_2 does act as a barrier to growth, further decomposition of L_1 takes place by the further nucleation of more α -crystals which may be similarly surrounded by L_2 , and so on, until eventually the α and L_2 phases are present in proportions given by the lever rule. Upon further cooling of the alloy liquid L_2 deposits some more α phase onto the existing α crystals until finally the lower transformation temperature is reached, whereupon the remaining

liquid freezes by an eutectic (or sometimes a peritectic) reaction [25]. The microstructure of a monotectic alloy, which is frozen free-directionally, is characterized by a spherical solid cell and separated L_2 phase lying along its radii [2].

2.4.3. Progressive or, Steady State, Monotectic Freezing

The distribution of the monotectic reaction products are randomly arranged when solidification is allowed to proceed normally. As with eutectic alloys the product phases in monotectic alloys can be distributed in a regular geometrical pattern when the alloy is frozen under steady-state conditions.

Consider the monotectic alloy in Fig. 2.15, frozen directionally in a vertical mold at a constant freezing rate as seen in Fig. 2.16. When the temperature gradient is moved upwards along the mold, the temperature of the alloy at the bottom of the mold drops to T_m and solid α can deposit from L_1 . For simplicity the solid-liquid interface can be assumed to be planar. The liquid adjacent to the interface is enriched in B due to solute rejection and it therefore becomes supersaturated with respect to L_2 , and droplets of L_2 nucleate to relieve supersaturation [21]. At this point the important question is, where the second phase will nucleate. The answer depends on the relative values of $\gamma_{L_1L_2}$, $\gamma_{S_1L_1}$ and $\gamma_{S_1L_2}$, the interfacial energies per unit area between the two liquid phases L_1 and L_2 , the solid S_1 and L_1 , and S_1 and L_2 , respectively. Fig. 2.17 shows schematically the position regarding the nucleation behavior for different selective values of three interfacial energies. If the relation between the magnitudes of the interfacial energies are such that as in Fig. 2.17(a),

$$\gamma_{S_1L_1} > \gamma_{L_1L_2} + \gamma_{S_1L_2}$$

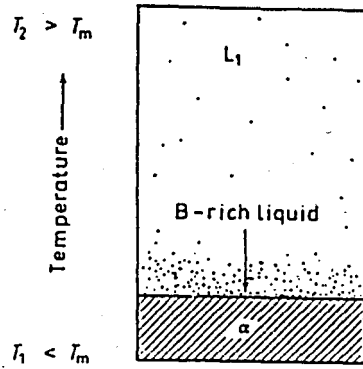


Fig. 2.16. Schematic drawing of unidirectional freezing of an alloy of monotectic composition, with freezing from bottom to top, showing initial deposition of α -phase [21].

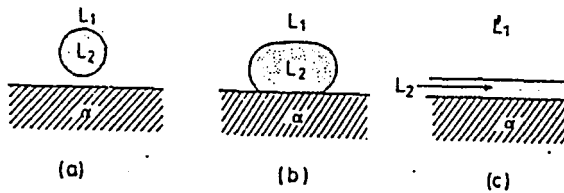


Fig. 2.17. The nucleation behavior of liquid L_2 (a) non-wetting, (b) partial wetting, (c) complete wetting [21].

In this case the second liquid phase L_2 will be unable to nucleate on the solid substrate and isolated droplets of L_2 must therefore nucleate within L_1 . What next happens to the droplets of L_2 will depend upon their buoyancy, they will float or sink depending upon the density differences of the two liquids at a velocity given by the Stoke's formula

$$V = (2/9)gr^2(D_1 - D_2)/\eta_1$$

where, r is the radius of droplets, D_1 is the density of L_1 , D_2 is the density of L_2 , η_1 is the viscosity of L_1 , and g is the gravitational constant [21].

As long as $V > R$, where R is the crystal growth rate, the droplets can escape from the region of the interface and float to the top of the melt. However, if $V < R$ trapping of the droplets in the solid may occur.

It is found that there is a critical velocity of the interface above which particles in suspension in the melt are taken into the solid, and below which the suspension is pushed along by the moving solid-liquid interface [22].

In Fig. 2.17(b) it is assumed the case where;

$$\gamma_{S_1L_2} < \gamma_{L_1L_2} + \gamma_{S_1L_1}$$

$$\gamma_{S_1L_1} < \gamma_{L_1L_2} + \gamma_{S_1L_2}$$

or,

$$\gamma_{S_1L_2} + \gamma_{L_1L_2} > \gamma_{S_1L_1} > \gamma_{S_1L_1} - \gamma_{L_1L_2}$$

The illustration actually represents the situation where;

$$\gamma_{S_1L_2} = \gamma_{S_1L_1} - \gamma_{L_1L_2} \cos \theta$$

For this case the interfacial energy conditions let L_2 droplets to nucleate on the solid substrate. Once an L_2 droplet has nucleated on the interface atoms of B that are rejected from the solid during growth, diffuse to the drop of L_2 , which elongates in the growth direction simultaneously with the growth of the solid. Steady state conditions can be achieved as shown in Fig. 2.18, in much the same way as steady state eutectic solidification, except that in monotectic freezing one of the products of the reaction is another liquid phase. On cooling from the monotectic temperature to the eutectic temperature (Fig. 2.15), liquid L_2 deposits some S_1 from the solution, this additional S_1 deposited on the existing S_1 at the periphery of the L_2 cylinders which therefore decrease slightly in thickness along their length during cooling. The cylinders of liquid L_2 finally solidify according to the reaction at lower temperatures (eutectic or peritectic)

at a large distance behind the main solid liquid interface [21]. Because of small diffusion distances involved within each cylinder of L_2 , the products of the low temperature reaction separates completely, solid S_1 being deposited on to the S_1 already present, leaving S_2 as a continuous central fiber. The phase separation that is, the average distance between the centers of neighboring fibers of S_2 , in such monotectic systems has the similar functional dependence on growth rate as in eutectic systems as $\lambda = R^{-n}$ where λ is the phase separation and $n \approx 0.5$.

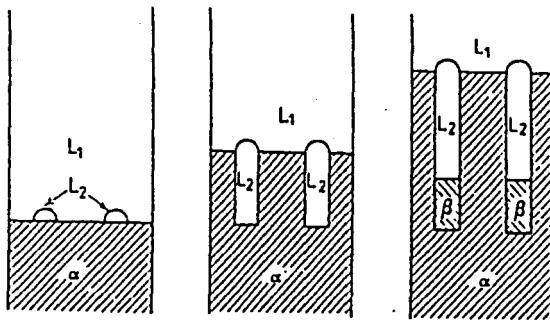


Fig. 2.18 Schematic drawing of unidirectional growth of the monotectic alloy [21].

Chadwick [21] stated that the only necessary condition for the formation of a duplex structure from a monotectic reaction is therefore, that the wetting angle θ of L_2 on S_1 must be less than 180° and greater than 0° in the presence of L_1 . But, Cahn [23] stated that the thickness of the film of the intruding wetting liquid is a function of a pressure called the disjoining pressure. It represents the work done in moving the two non-contacting phases closer together and in the limit of zero intruding film thickness it represents the work done in creating the surface of direct contact with its higher free energy. And composites can be grown even if L_2 is a non-wetting liquid if the growth velocity is large enough to overcome the disjoining pressure.

If the wetting angle θ of L_2 on S_1 in the presence of L_1 is 0° as in Fig. 2.17(c) or if the wetting angle of L_2 on S_1 in the presence of L_1 is

180° and L_2 has a higher density than L_1 , a layer of L_2 will seal the solid from L_1 and steady state growth will be impossible. In this case the solidification process would probably involve the intermittent freezing of S_1 ahead of the L_1L_2 interface leaving the liquid layer of L_2 to freeze subsequently [21].

Cahn [23] also predicted the theoretical considerations of temperature dependencies of the surface energies. The difference between the critical and monotectic temperatures (i.e. the height of the miscibility gap) shows whether the system will be wetting or non-wetting. Monotectic systems having relatively lower miscibility gap are usually non-wetting systems.

Composite growth of monotectics depends on the following factors; (1) whether the second liquid phase wets the solid phase or not; (2) the relative densities of the two liquids; (3) the rate of solidification and, (4) the direction of solidification [1, 23-26]. Composite structures have been achieved in a number of monotectic alloy systems, but the experimental data concerning the necessary growth conditions have proved contradictory. It has been proposed by Livingstone and Cline [27] that the structure which occurs, composite or dendritic, is the one that grows faster at a given undercooling (or, equivalently, the one that grows with less undercooling at a given growth rate), and composite-dendritic transition moves further from the monotectic composition as growth rate increases. But, Toulou et al [24] stated that with increasing growth rate and decreasing gradient the microstructures show transitions from regular rod-like arrangements of the lower melting point phase, through arrays of aligned droplets to coarse droplet dispersions.

For example, the study of the monotectic systems with a low miscibility gap (e.g. Cu-Pb, Cd-Ga) by Kamio and Oya [2], by

Livingstone and Cline [27] and by Grugel et al [1, 27] over a range of compositions around the monotectic have indicated that irregularly branched rod microstructures develop at high growth rates otherwise degenerating into discontinuous globular structures. However, in an alloy with a higher miscibility gap (e.g. Al-In) regular rod microstructures were obtained at slow growth rates, transforming with increasing growth rate to arrays of aligned spherical droplets and finally degenerating into irregular globular dispersions [24]. But it is also demonstrated by Grugel et al [1] that ternary additions to the system may alter the height of the miscibility gap and changes the composite growth behavior of the system.

Also post-solidification (ripening) effects as observed in eutectics, affects the microstructure of the monotectic alloys [24]. Indeed this effect is likely to be more pronounced since the minor rod phase remains liquid behind the solidification front thus, allowing a more rapid diffusional path for the ripening process, and causing the rod-like structure to breakdown and degenerate.

Ripening effects subsequently cause spheroidisation into regularly spaced droplet arrays. This sequence of events is diagrammatically illustrated in Fig. 2.19. If an oscillation develops at the monotectic growth front, the wavelength of the perturbations introduced along the length of the rods, λ_p , will be related to the frequency of the oscillation, f , and the growth velocity, V , as $\lambda_p = V/f$ [24].

2.5 The Zn-Bi System

The equilibrium phase diagram of Zn-Bi system is shown in Fig.2.20. In this system the critical temperature is 878 °K (605 °C) and monotectic reaction takes place at a temperature of 691 °K

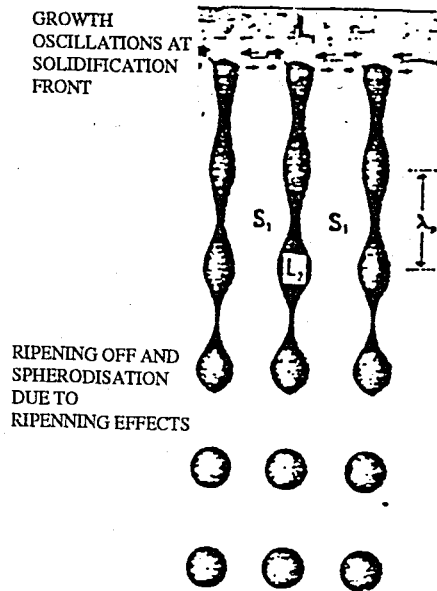


Fig. 2.19. Diagrammatic illustration showing how growth front oscillations combined with post solidification effects caused degeneration of a rod-like composite into an aligned droplet array [24].

(428 °C) and a composition of 0,6 at.% (1.9 wt.%) Bi. And, the eutectic reaction takes place at 527.5 °K (254.5 °C). In order to evaluate the possible pathways of the microstructural evolution in Zn-Bi system, the determination of the metastable phase diagram of this system by the thermodynamic calculation must be done [28]. These include the metastable extrapolation of the binodal and spinodal lines for liquid and a determination of equal free energy curve (T_0) between solid and liquid. Representative free energy curves of liquid and solid at 500 °K are shown in Fig. 2.21. The two curves intersect in the Zn-rich end marking the equal free energy condition. Fig. 2.22 shows the metastable extension of the liquid phase field (binodal), liquid spinodal and T_0 of liquid and solid solution at the Zn-rich end. The dotted curve superimposed on it to denote undercooling required for homogenous nucleation of second liquid (L_2). At all temperatures of interest below the melting point of Zn, the solid solution is unstable at all compositions (i.e. there is no solid solubility between Zn and Bi) [29].

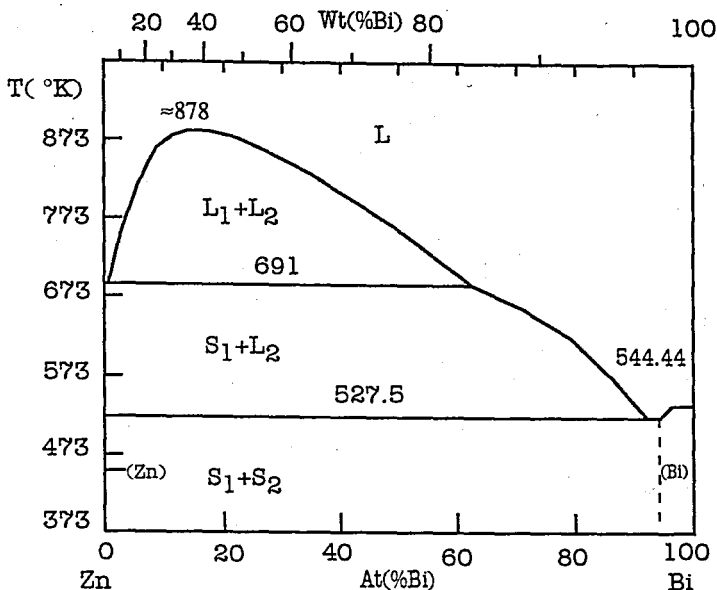


Fig 2.20. Equilibrium phase diagram of Zn-Bi system [28].

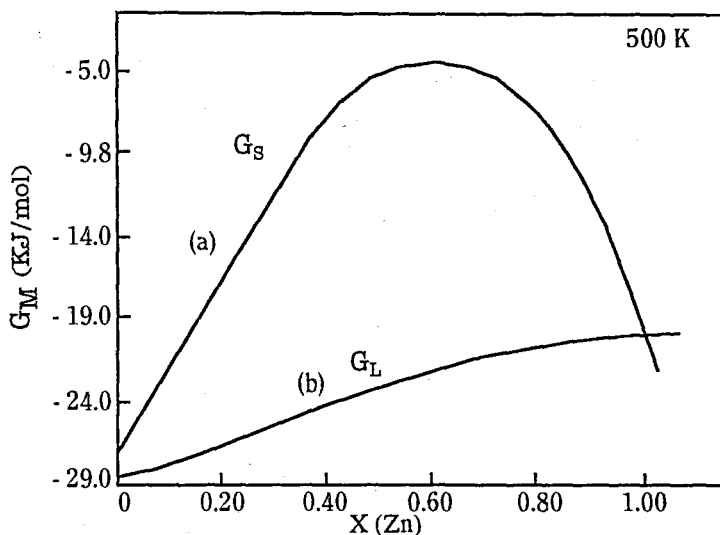


Fig. 2.21. Variation of free energy per mole as a function of composition (X_{Zn}) at 500 °K: (a) solid solution (G_S); (b) liquid solution (G_L) [28].

Relatively little information about Zn-Bi system is available in the literature as for most of the other monotectic alloys. Carlberg et al [6] studied the influence of microgravity on solidification, Goswami et al [29] studied the microstructural evolution and transformation pathways during rapid solidification and Toloui et al [24] studied the microstructural perturbations in directional solidification of Zn-Bi

system. Microstructures of Zn-Bi alloys cast under microgravity with various compositions are shown in Fig. 2.23. In the study of Toloui et al [24] Zn-Bi system is found to act in a similar way to the other monotectic systems having a high miscibility gap (i.e. wetting systems). Monotectic temperatures, height of miscibility gaps and freezing ranges of some monotectic systems and the Zn-Bi system are tabulated in Table 2.5. The system at present has no industrial application but, because of its relatively low critical and monotectic temperatures with respect to other monotectic systems it is chosen as a model system to monotectics.

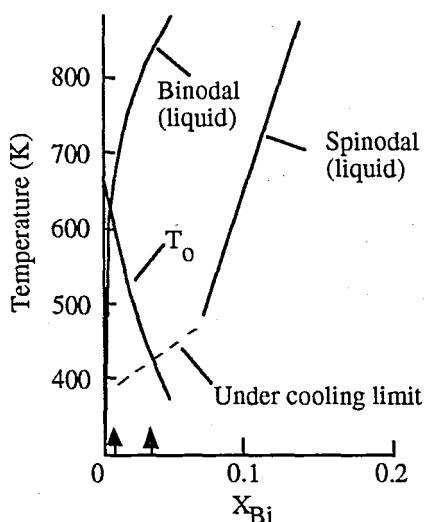


Fig. 2.22. Phase diagram of Zn-Bi system, showing metastable extension of liquid phase field (binodal), liquid spinodal and T_0 of liquid and solid solution at Zinc-rich end, dotted curve denotes undercooling required for homogenous nucleation of L_2 [28].

Table 2.5 Monotectic temperatures (T_m), height of miscibility gaps ($T_c - T_m$) and freezing ranges ($T_m - T_e$) of some monotectic systems [29].

Alloy	T_m (°C)	$T_c - T_m$ (°C)	$T_m - T_e$ (°C)
Al-Bi	657	400	386
Al-In	637	150	481
Pb-Zn	417	370	100
Cd-Ga	282	13	253
Cu-Pb	952	48	626
<u>Zn-Bi</u>	<u>416</u>	<u>400</u>	<u>162</u>

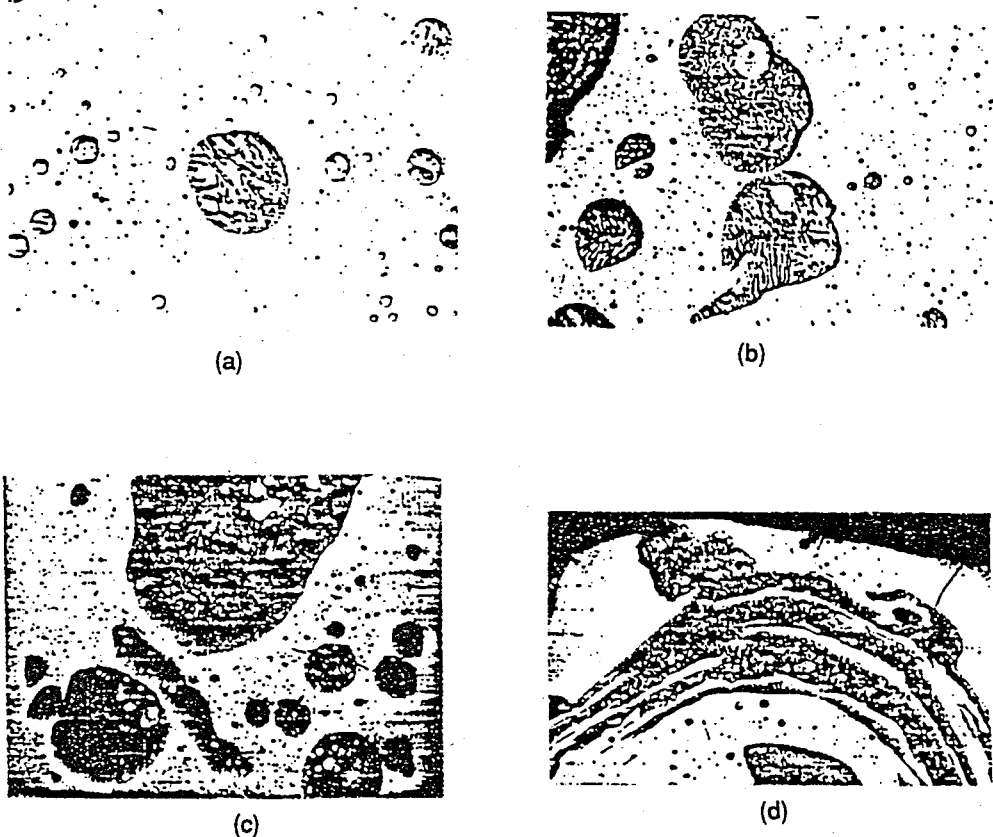


Fig. 2.23. Microstructures of (a) Zn-0.03wt%Bi (x168), (b) Zn-0.07wt%Bi (x28), (c) Zn-0.09wt%Bi (x11), (d) Zn-0.17wt%Bi (x11) cast under microgravity conditions [6].

2.6. Squeeze Casting of Monotectic Alloys

It is the knowledge of the author that the only reference about the squeeze casting of monotectic systems in the current literature is the Epanchintsev's study [30] of hypermonotectic Cu-Pb alloy. He reported a two fold increase in tensile strength, elongation, hardness and impact strength over gravity cast values, when pressures of 150-300 MPa were applied to the Cu-20%Pb hypermonotectic alloy during solidification.

Table 2.6. Effects of squeeze casting on the wide freezing range alloys [14].

Alloy (wt.%)	$T_L - T_s$ (°C)	Method	Density (g cm ⁻³)	HB	σ_{TS} (MPa)	ϵ_f (%)
Zn-27%Al	110	Not squeezed	4.91	60	290	3.6
		Squeezed	5.42	77	493	12.3
Al-20%Si	85	Not squeezed	2.44	69	90	2.5
		Squeezed	2.63	80	113	4.5
Al-7%Si	35	Not squeezed	2.24	35.5	73	3.5
		Squeezed	2.55	42.7	96	7
Al-5%Mg	50	Not squeezed	2.61	50	55	5
		Squeezed	2.63	60	185	25
Al-10%Mg	150	Not squeezed	2.51	70.5	97	5
		Squeezed	2.58	78.4	260	26
		Squeezed and annealed	2.68	82	315	27
Al-4.5%Cu-0.5%Bi	90	Not squeezed	2.69	40	165	14
		Squeezed	2.80	49	185	21
		Squeezed and annealed	2.80	64	251	23
Fe-3%C-2%Si	180	As-received	2.99	93	360	37
		Sand cast	7.08	145	145	3
		Not squeezed	7.19	135	229	2.5
		Squeezed	7.46	215	410	5.5

It is reported by Savaş and Altıntaş [14] that squeeze casting method improves the mechanical properties of wide freezing range binary alloys. Table 2.6 shows the comparative properties of some wide freezing range binary alloy castings for squeezed and not squeezed conditions. But, Rolland et al [31] noted that if the pressure is not sufficiently high to increase the grain size, strain induced macrosegregation may occur especially in the central part around the hot spot of the castings causing a non-homogenous microstructure. And, this tendency for macrosegregation increases with increasing pressure and decreasing alloying content for insufficient pressures.

III. EXPERIMENTAL STUDY

3.1. Dies and Materials Used

Melts of pure zinc and Zn-1.9wt.%Bi monotectic alloy were prepared using commercial grade zinc ingots of 99.95 % purity and, bismuth shots of 99,99 % purity.

For the production of squeezed and not squeezed castings and cooling curve measurements the dies and the punches made of mild steel were used. In Figs. 3.1 and 3.2 the dimensions of the dies and the punches of two different designs are shown.

In determining the temperatures for cooling curve measurements K-type (Ni-CrNi) thermocouple wires of 0.5 mm diameter were used. The wire diameter was chosen as small as possible in order to reduce the response time.

3.2. Melting and Casting Practice

3.2.1. Preparation of Castings

For all castings, alloys of 500 g in total weight were prepared. Zinc slices from ingots of 490.5 g and bismuth shots of 9.5g were weighed to obtain the monotectic composition of Zn-1.9wt.%Bi. Also 500 g castings of pure zinc were prepared for comparison purposes and to see the effects of bismuth addition on various properties. An electronic precision balance of 0.01g. accuracy was used to weigh the components.

In alloy preparation first, zinc was melted in a graphite crucible and kept molten at 600 °C in an electric resistance furnace. Following this, bismuth was added to the melt under argon atmosphere to prevent the oxidation of bismuth. During addition of bismuth and before pouring the melt into the die, the melt was stirred in order to provide a homogeneous molten alloy.

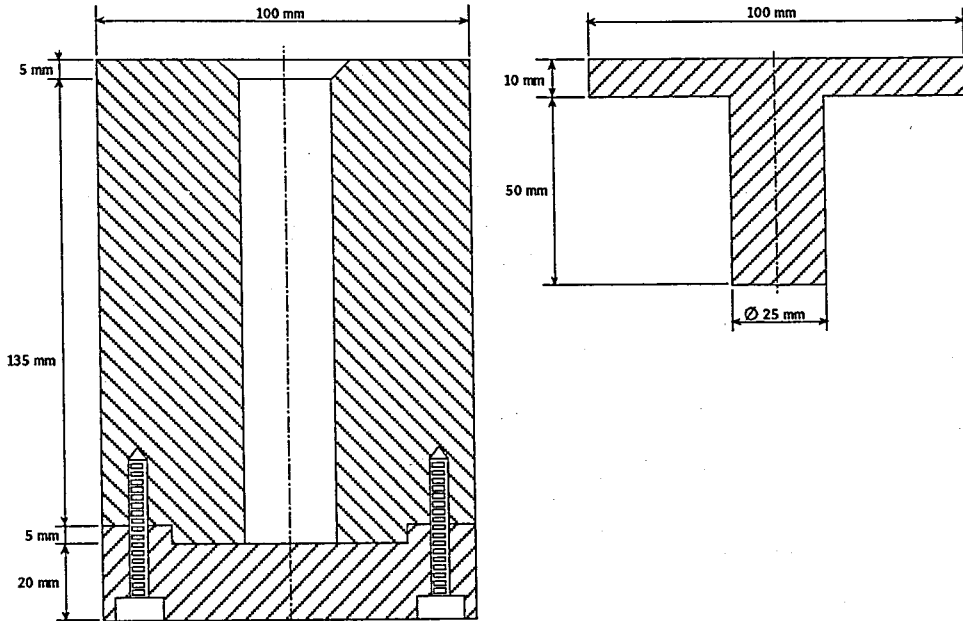


Fig. 3.1. Squeeze casting die used for the production of castings.

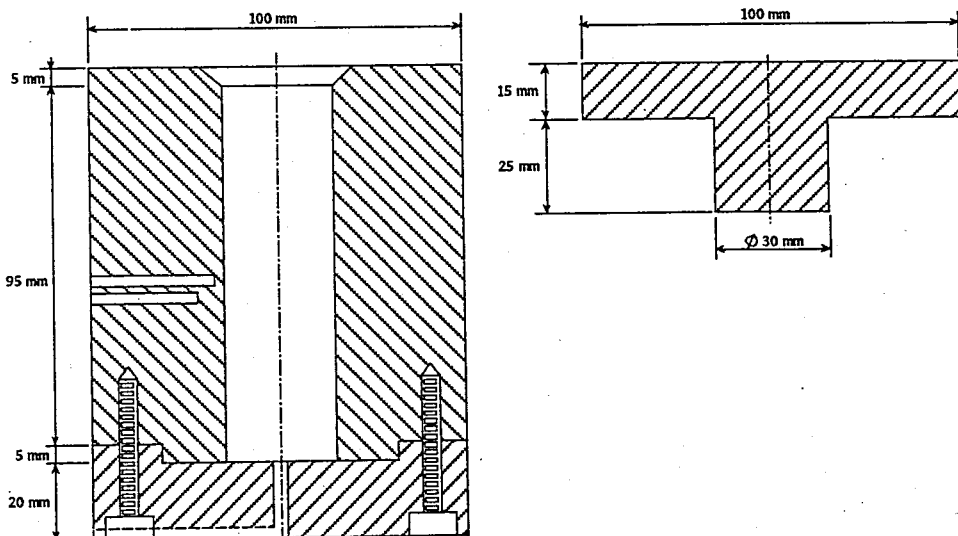


Fig. 3.2. Squeeze casting die used in determination of cooling curves.

3.2.2. Squeeze Casting

The casting process was repeated under five different conditions for five different groups of Zn-Bi monotectic alloy and, two different conditions were used for pure zinc. Five specimens for each group were produced. The castings were grouped according to the casting conditions as follows:

(i) For Zn-19% Bi monotectic; (1) not-squeezed (cold die, die at 20 °C); (2) not-squeezed (hot die, die at 250 °C); (3) squeezed at 50 MPa; (4) squeezed at 85 MPa; (5) squeezed at 120 MPa.

(ii) For pure zinc; (1) Not-squeezed (hot die, 400 °C); (2) squeezed at 120 MPa.

Die temperatures were fixed at 250 °C during squeeze casting of Zn-1.9%Bi monotectic and, at 400 °C for pure zinc castings. The die temperature for Zn-Bi alloy was selected near the eutectic temperature of the system because, it was thought that the higher temperatures might result in gravitational segregation of the heavy bismuth-rich liquid and lower temperatures would leave no time for the squeeze casting process.

For group 1, the alloy melt which was prepared in a manner explained in section 3.2.1 was poured into the die at room temperature (20 °C) and, it was allowed to freeze freely in its die.

For groups 2-5, the die and the punch were preheated in an electric resistance furnace up to 250 °C and kept at this temperature for thermal equilibrium to be reached then, taken out of the furnace. The inner surface of the die was painted using fine graphite mixed with water. For group 2, after the melt was poured into the die it was

allowed to freeze freely. But in groups 3-5, after pouring the melt, the die was immediately placed in a hydraulic press, which was set to the desired pressure before (i.e. either, 50, 85, or 120 MPa). Then, the punch was taken out of the furnace and placed on top of the melt in the die. As soon as the melt cooled down to its freezing range (i.e. approximately 15-20 seconds after pouring the melt for Zn-1.9wt%Bi monotectic) the squeezing pressure was applied until the casting solidified completely (for about 2 minutes). The set-up for the squeeze casting process is shown in Fig. 3.3. And, in Fig. 3.4 two castings which were produced by gravity casting and squeeze casting methods are shown.



Fig. 3.3. Squeeze casting set-up.



Fig. 3.4. Castings produced by gravity casting (at left hand side) and, by squeeze casting (at right hand side) methods.

Fig. 3.3. Schematic representation of the experimental set-up used in cooling curve determination.

3.3. Cooling Curve Determination

The squeeze casting die, shown in Fig. 3.2 was used for the cooling curve measurements. For temperature measurement the thermocouple compensation cables of the K-type were used. The calibration of the thermocouples were done at 0 °C (water+ice mixture), at 327 °C (solid-liquid transition temperature of lead) and at 419 °C (solid-liquid transition temperature of pure zinc). Millivolt readings corresponding to these values were found and calibration curves for thermocouples were drawn.

During freezing, measurements were taken at three different locations at the same time. The experimental set-up for the cooling curve measurement is shown in Fig.3.5. Thermocouple no.1 was placed at the center of the die cavity to record the temperature of the melt. It was placed inside a ceramic tube and its hot junction was about 5 cm distance from the bottom end. Thermocouple no.2 was placed in the die, 1 mm from the die-melt interface at the same height as no.1, to record the temperature variations at this interface. And, thermocouple no.3 was placed in the die, 5 mm from the die-melt interface to record the temperature values of the die.

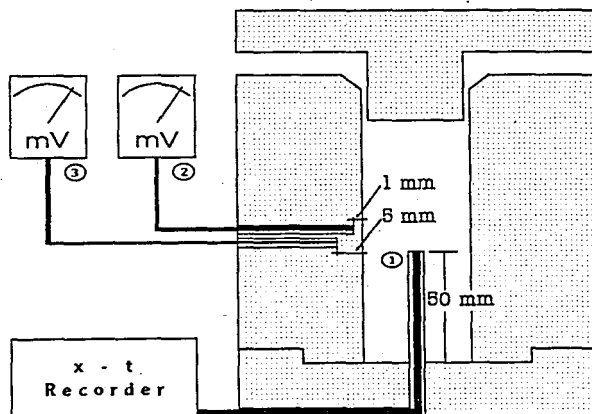


Fig. 3.5. Schematic representation of the experimental set-up used in cooling curve determination.

Thermocouple no.1 was connected to an (X-t) chart recorder, no.2 and 3 were connected to two millivoltmeters. Two measurements were done for not-squeezed (hot die) and squeezed (120 MPa) castings to see the difference in cooling rates. Both measurements were repeated twice. Millivolt values from the two millivoltmeters were read and recorded simultaneously in every 5 seconds. Then, the millivolt values were converted to degrees centigrade by using the calibration charts of the thermocouples.

3.4 Chip Length Measurement

While machining tension test specimens from all the seven groups of castings the chips were collected to see any effect of bismuth addition and pressure application on the machinability of the specimens. The depth of cut (a), feed (s) and the corner radius (r) were kept as constant parameters as follows:

Depth of cut : $a=1.0$ mm

Feed : $s=0,1$ mm

Corner radius : $r=0,4$ mm

Four cutting speeds (n) 355, 500, 700 and 1000 rpm were chosen for the examination. The equivalent tangent cutting speeds were calculated by using the formula $V=\pi dn/1000$ where, V is the tangent cutting speed (m/min), d is the outer diameter of the test bar (22 mm), and n is the angular speed.

The chips were classified and their lengths were measured by using a ruler for pure zinc specimens and, under a microscope (either, at x40 or x80 magnification) for the finer chips of Zn-Bi alloy specimens.

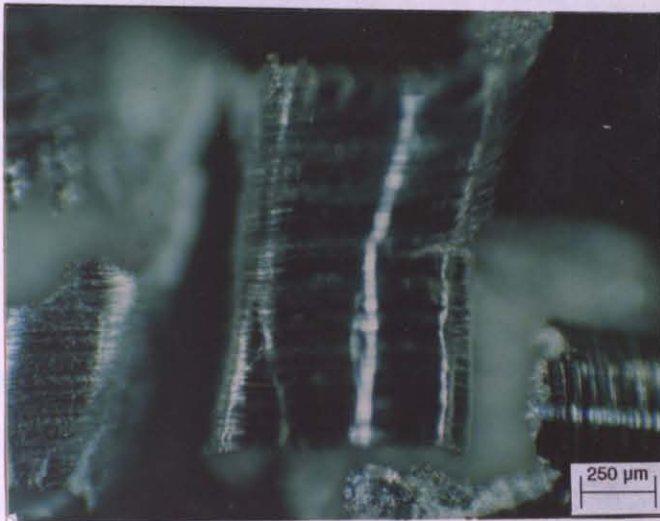


Fig. 3.6. An enlarged view of the chip resulted from a squeeze cast Zn-Bi specimen ($P=85$ MPa, $\times 40$ magnification, $V=69$ m/min).

3.5. Tensile Testing

Three specimens from each group were taken and machined to a substandard size for tensile testing according to the ASTM B557M standard as shown in Fig. 3.7 [32].

Specimens were fractured in an Instron model 1186 universal tensile testing machine using a crosshead speed of 5 mm/min and a maximum load of 10 kN. Load versus time graphs were recorded using an X-t chart recorder.

3.6. Density Measurement

The densities of the specimens were measured in order to calculate the amount of porosity in castings. In the density measurements ASTM D792 standard method A was used [33]. By using a proper set-up the specimens were held by a fine wire, weighed and submerged in pure water. While it was in the water it was weighed again. The first measurement gave the mass and the difference between the two

measurements gave the volume of the specimens. The densities were calculated from these values. In the measurements an electronic balance of 0.01 g. accuracy was used.

One specimen from each seven group was taken out for optical metallography and hardness tests. Half of a specimen was machined longitudinally in a milling machine. Then, the specimens were polished on waterproof SiC abrasive papers of 180, 360, 1000 and 1800 grades and, finally, on alumina paste. A 50% HCl and water mixture was used as macro-etchant [34] and the photographs were taken by macro lenses using a photomicrographer.

3.7.2. Microstructural Examination

Macro etched specimens were polished again on waterproof SiC papers of 360 and 1800 grades and then, on alumina paste. The specimens were placed under an optical microscope and photographs were taken under magnifications from 100 to 1000 \times .

3.8. Hardness

The same specimens prepared for metallography were also in hardness tests. In Vickers hardness tests, the specimens were indented under a 2 kg load by using a Vickers hardness tester. The measurements were taken along the centerline on a line 8 mm from the centerline of the specimen.

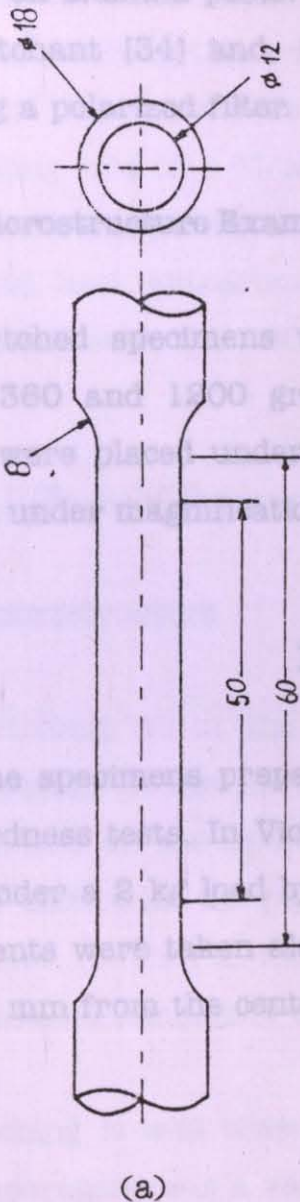


Fig. 3.7 (a) dimensions, (b) actual view of the tension test specimen.

3.7. Optical Metallography

3.7.1. Macrostructure Examination

One specimen from each seven group was taken out for optical metallography and hardness tests. Half of a specimen was machined longitudinally in a milling machine. Then, the specimens were polished on waterproof SiC abrasive papers of 180, 360, 1000 and 1200 grades and, finally on alumina paste. A 50% HCl and water mixture was used as macro-etchant [34] and, the photographs were taken by macro lenses using a polarized filter.

3.7.2. Microstructure Examination

Macro etched specimens were polished again on waterproof SiC papers of 360 and 1200 grades and then, on alumina paste. The specimens were placed under an optical microscope and photographs were taken under magnifications from x320 to x800 without etching.

3.8. Hardness Test

The same specimens prepared for optical metallography were used also in hardness tests. In Vickers hardness tester the specimens were indented under a 2 kg load by using a diamond pyramid indenter. The measurements were taken along the centerline of the casting and also on a line 8 mm from the centerline in every 10 mm intervals.

IV. RESULTS AND DISCUSSION

4.1. Effects of Pressure on the Cooling Rates of Castings

Cooling curves were obtained as explained in section 3.3. Figs. 4.1-4.3 shows the T-t curves recorded from respectively, the center-line, die-melt interface and die during freezing of two Zn-Bi monotectic castings. As can be seen from these figures application of pressure highly effects the heat transfer conditions during casting process. The average cooling rate of the melt in squeezed sample can be found from the slopes of the curves as 18 °C/sec. When compared with the average cooling rate of 8 °C/sec for the not-squeezed sample it is clear that squeeze casting promotes the intimate contact between casting and die for rapid heat extraction. Whilst the not-squeezed casting was solidified in 240 secs, the 120 MPa pressure lowered the freezing time to 70 secs.

4.2. Effects of Pressure on Macro- and Microstructures

4.2.1. Macrostructure

Before etching, all of the samples have found to have a central shrinkage piping. In the not-squeezed specimens the pipings were on the top portion of the specimens. As the squeezing pressure was applied and increased, the pipings were found to move away from the punch end and reduced in size. In the 120 MPa-squeeze cast specimen the piping almost completely disappeared.

After etching it was observed in the not-squeezed specimens that, the die temperature was a very important parameter on grain size and type. In Fig. 4.4 macrostructures of not-squeezed specimens are shown. In the not-squeezed cold-die sample the grains were very fine

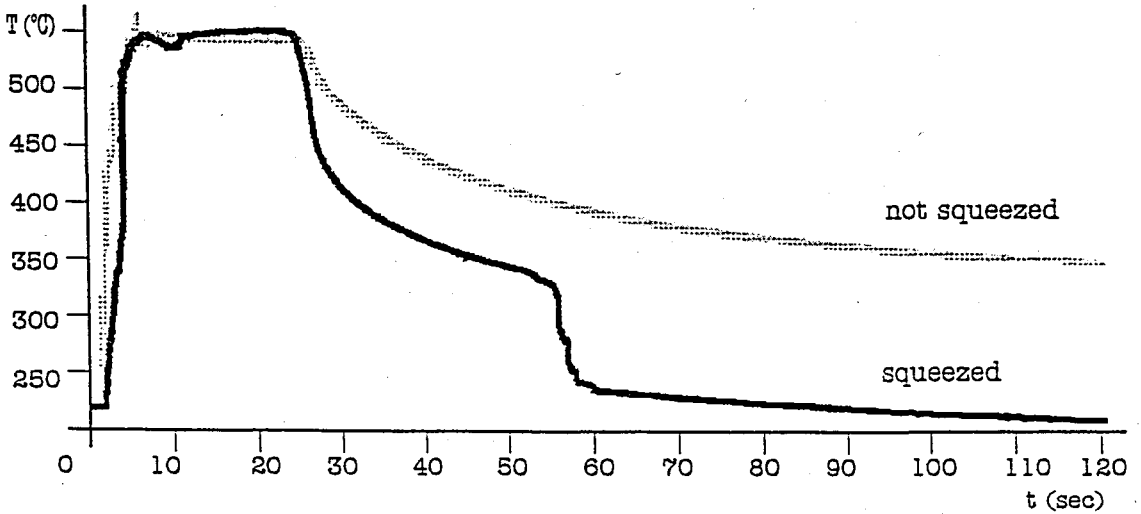


Fig. 4.1. Cooling curves recorded from the melt at the die centerline location during squeeze casting and gravity casting.

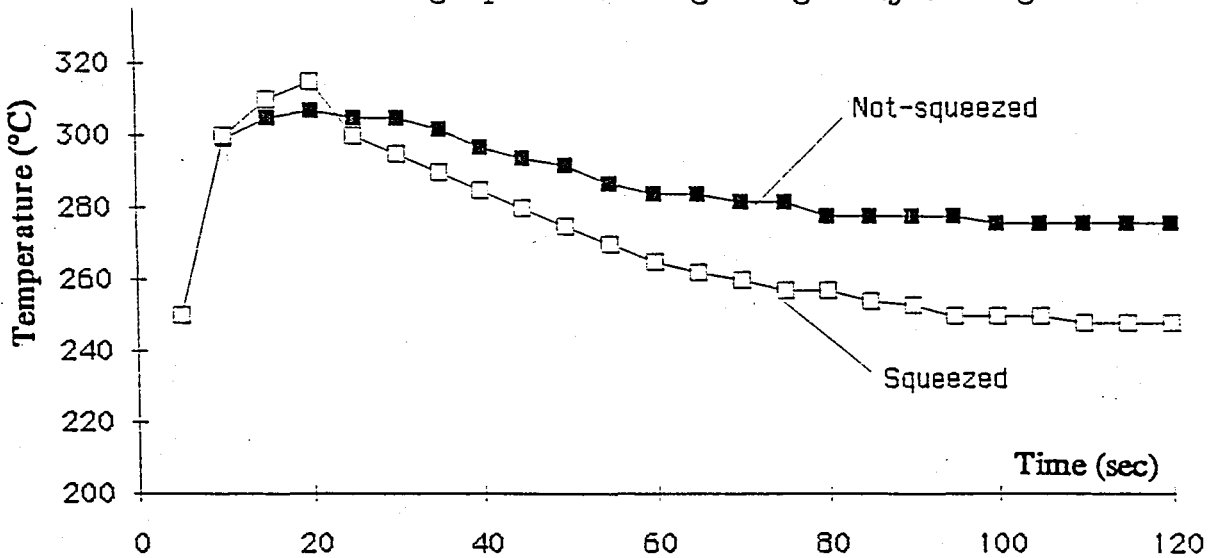


Fig. 4.2. Cooling curves for the melt-die interface for squeeze casting

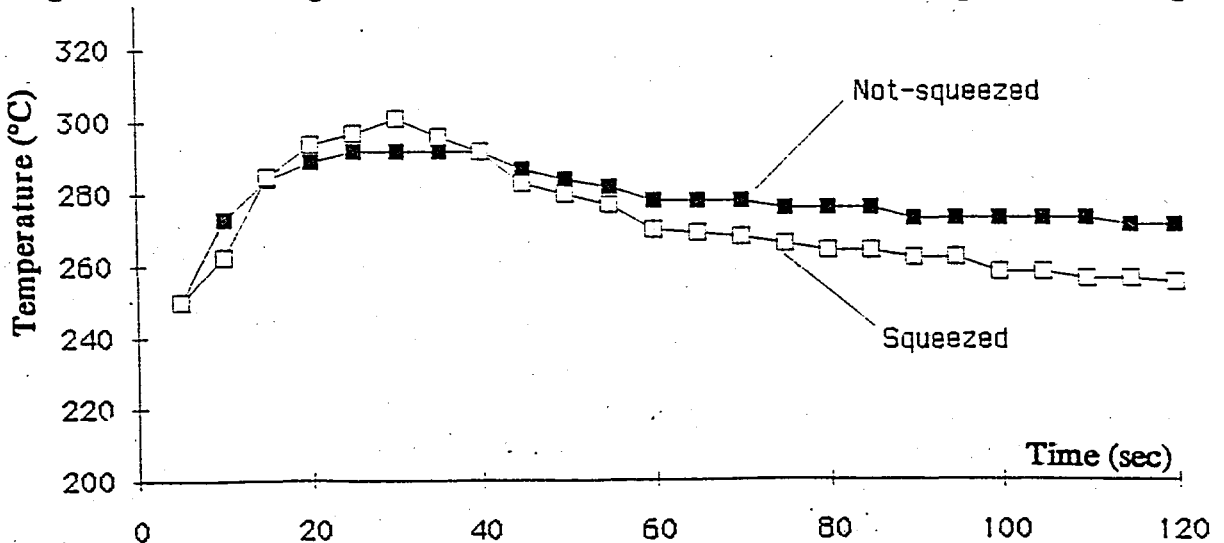


Fig. 4.3. Cooling curves for the die during squeeze casting and gravity casting.

as compared to the others. (Fig. 4.4(a)). The average grain diameter was found to be 0.66 mm. In the not-squeezed hot-die specimen coarser grains were exist, at the central part, an equiaxed zone was observed. The average grain diameter was measured as 1.42 mm (Fig. 4.4(b)).

in the middle portion of the specimens. The average grain diameter was found to be 1.57 mm in the 50 MPa-squeeze cast specimen and 1.08 mm in the 120 MPa-squeeze cast specimen. In Fig. 4.5 macrostructures of squeeze castings are shown. In Fig. 4.6 the change in average grain diameter as a function of casting position and in Fig. 4.7 the grain size variation along the longitudinal axis of squeeze cast specimens are plotted.

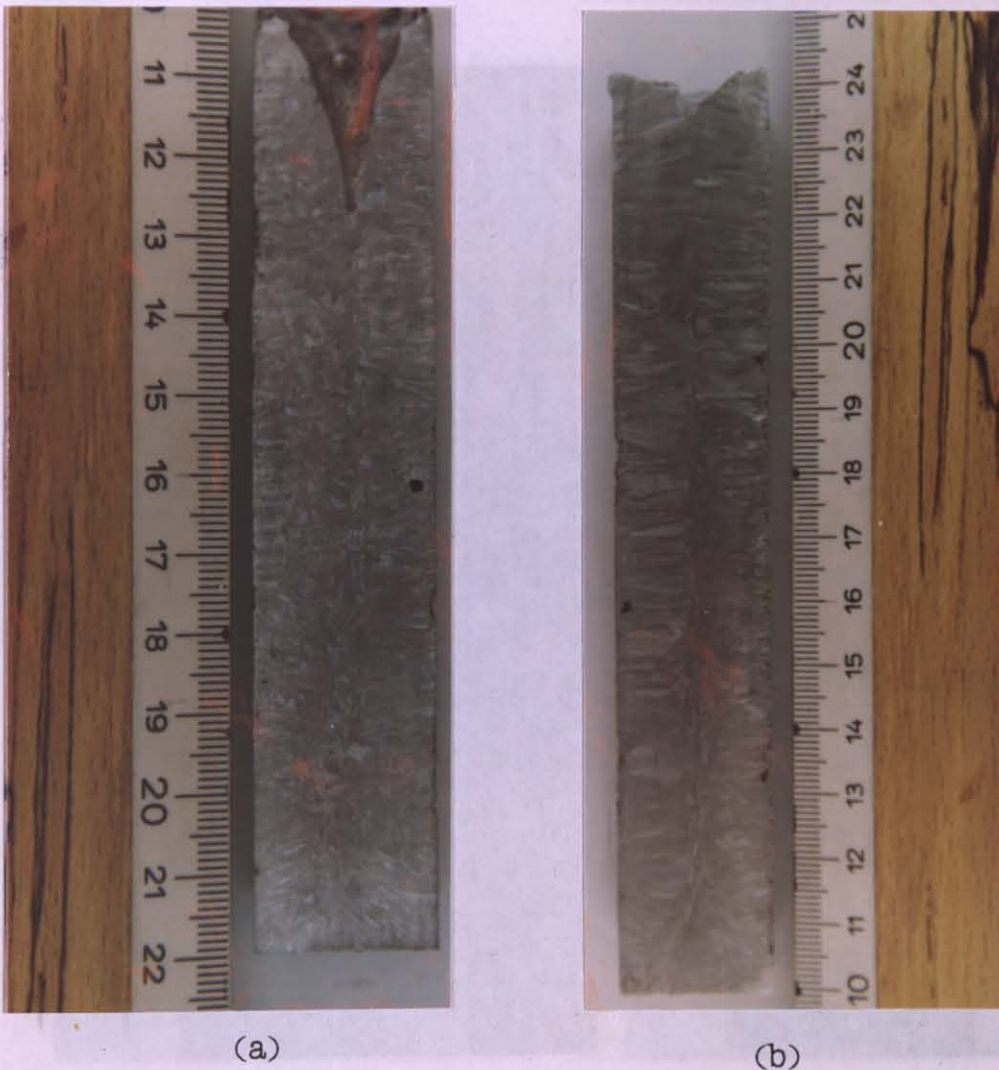


Fig. 4.4. Macrostructures of not-squeezed specimens cast into; (a) cold die at 20 °C, (b) hot die at 250 °C.

The equiaxed zone was narrower in the 50 MPa-squeeze cast sample and, was fully absent in the 120 MPa-squeeze cast sample. The grains were finer near the punch end and at the bottom and, were coarser in the middle portion of the specimens. The average grain diameter was found to be 1.57 mm in the 50 MPa-squeeze cast specimen and 1.08 mm in the 120 MPa-squeeze cast specimen. In Fig. 4.5 macrostructures of squeeze castings are shown. In Fig. 4.6 the change in average grain diameter as a function of casting condition and in Fig. 4.7 the grain size variation along the longitudinal axis of squeeze cast specimens are plotted.

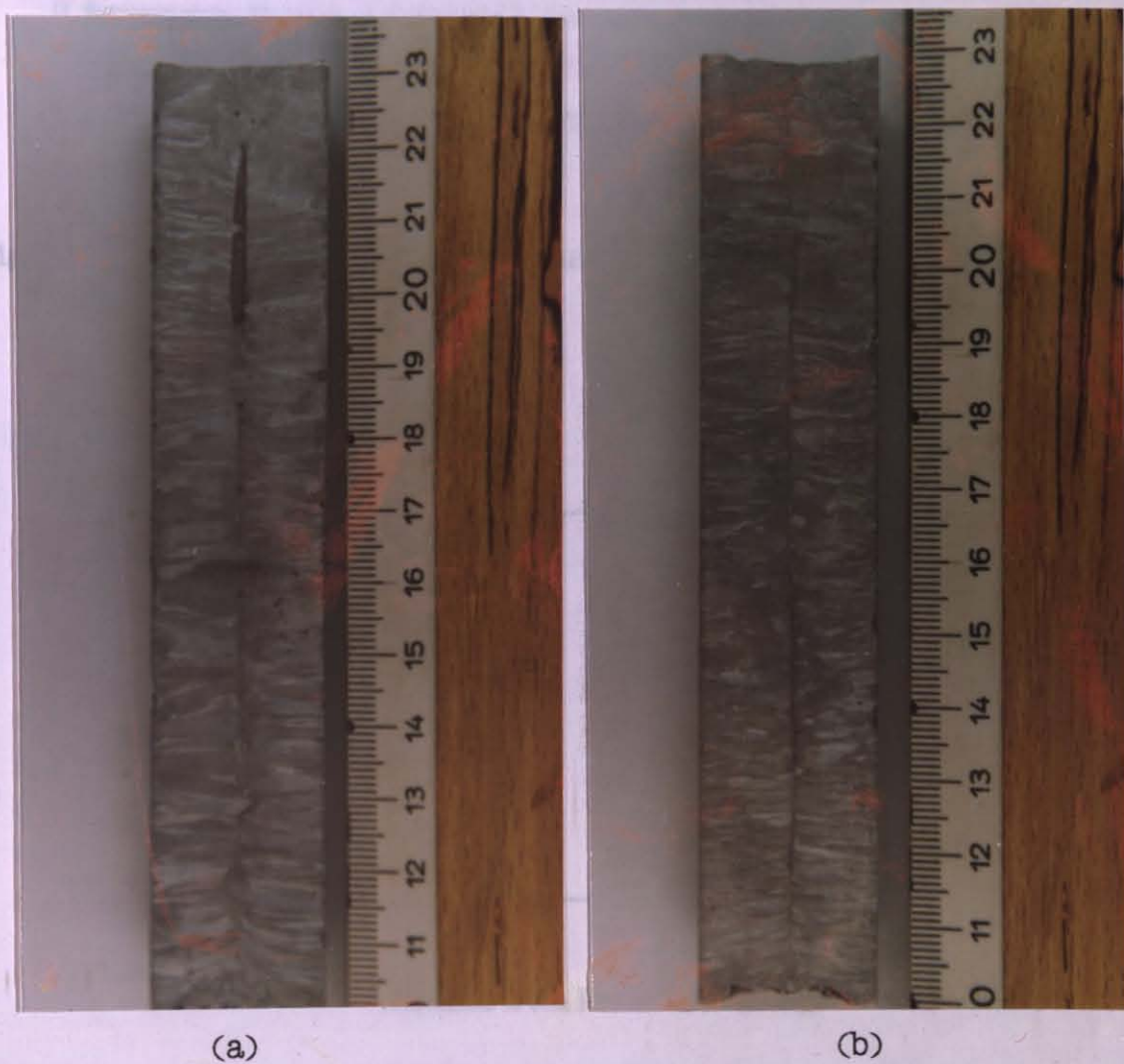


Fig. 4.5. Macrostructures of squeeze cast specimens squeezed under; (a) 50 MPa, (b) 120 MPa.

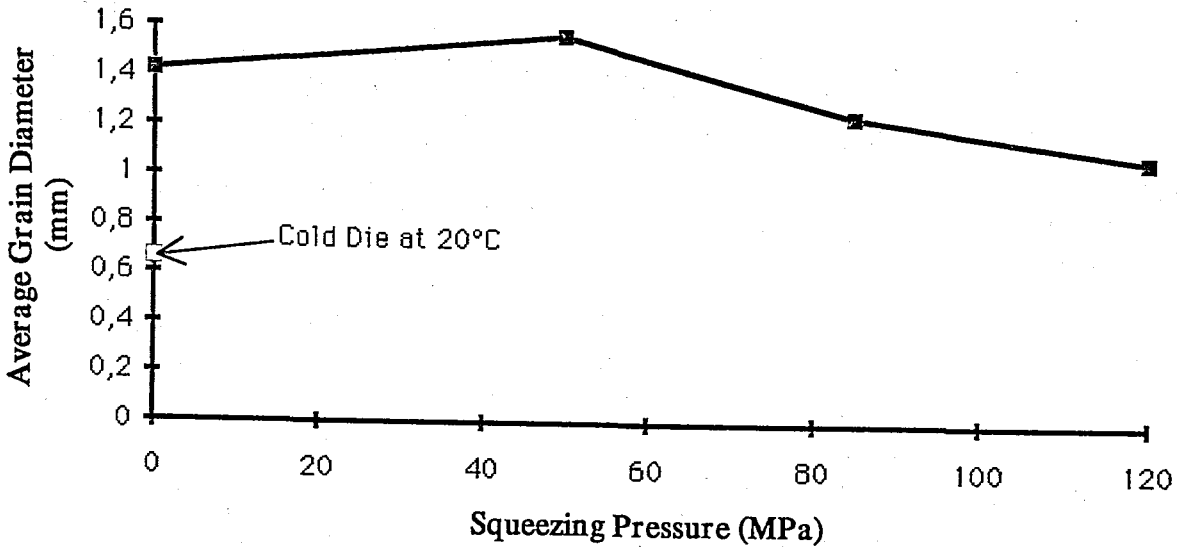


Fig. 4.6. Average grain diameter as a function of casting condition

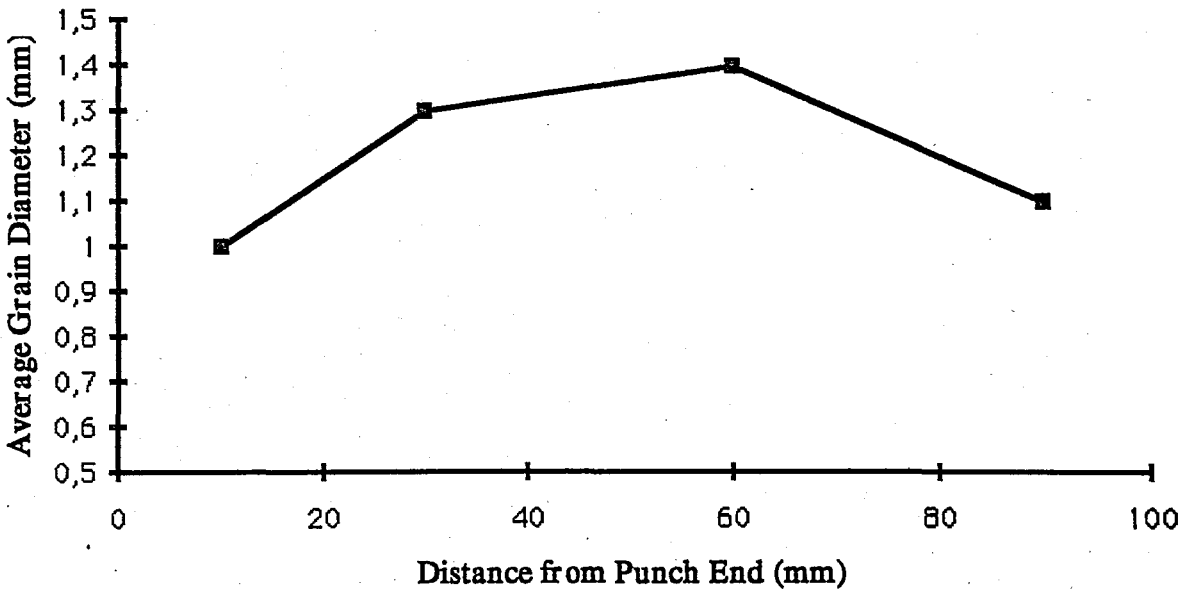


Fig. 4.7. Change in grain size along the longitudinal cross-section of 120 MPa-squeeze cast specimen.

4.2.2. Microstructure

In the microstructure examination the distribution of bismuth phase was found to be more uniform and at a finer scale in the not-squeezed samples. But, the porosity amount was higher than the squeezed samples. In Fig. 4.8 and 4.9 micrographs taken from the central part of the not-squeezed cold-die specimen are shown. The diameter of the largest bismuth particle was approximately 5 μm in this sample. The diameter of the pores were also in the same order in the same specimen and were distributed uniformly.

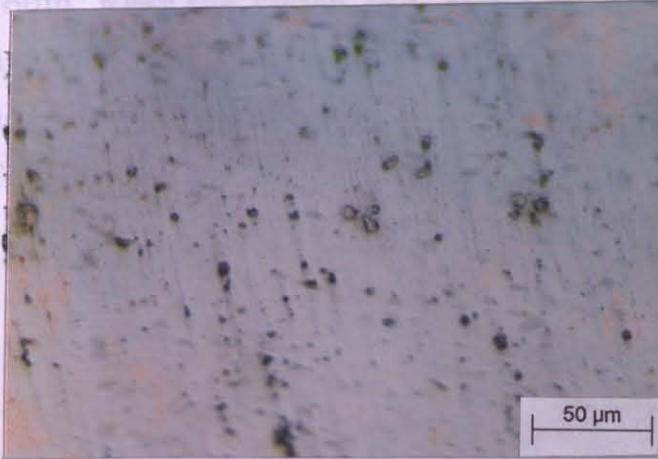


Fig. 4.8. Microstructure at the central part of a Zn-Bi monotectic specimen cast into cold die (20°C) and not squeezed (x320).



Fig. 4.9. Microstructure of the same region under a higher magnification (x800, oil lens).

In the squeezed samples, the maximum size of the bismuth particles are observed to increase in size around the centerline of the casting especially, near the hot spots in the sample. The bismuth particles were finer near surface edges. Also, the total porosity amount was decreased but, pores were gathered near the centerline and hot spots. The sizes of bismuth particles were observed to increase near hot spots and tended to decrease near casting surface. The maximum size of bismuth particles near the centerline was 5 times greater than the size of the particles in the not-squeezed sample and were 25-30 μm . Near the casting surface the maximum size of the particles were 5 μm . Near the punch end, along the centerline, the size of the bismuth particles were decreased and the maximum size of a bismuth particle was found to be 15 μm . In Figs. 4.10-4.13 micrographs of the 85 MPa-squeeze cast specimen are shown.

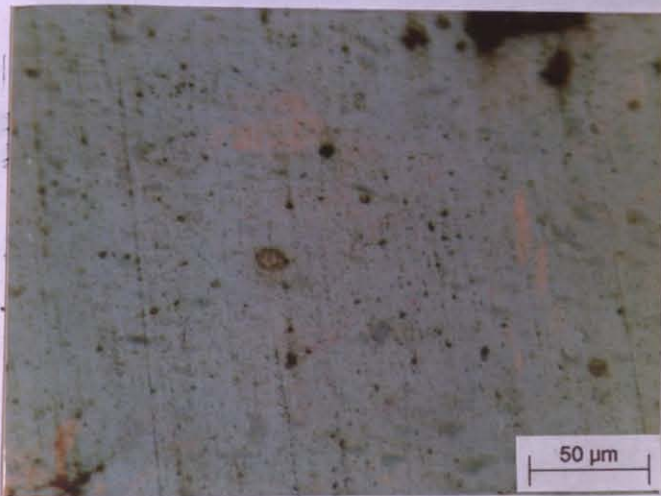


Fig. 4.10. Microstructure at the central part of a Zn-Bi monotectic specimen squeeze cast under 85 MPa (x320).



Fig. 4.11. Microstructure at 1.5 cm from bottom end of the specimen squeeze cast at 85 MPa (x800, oil lens).

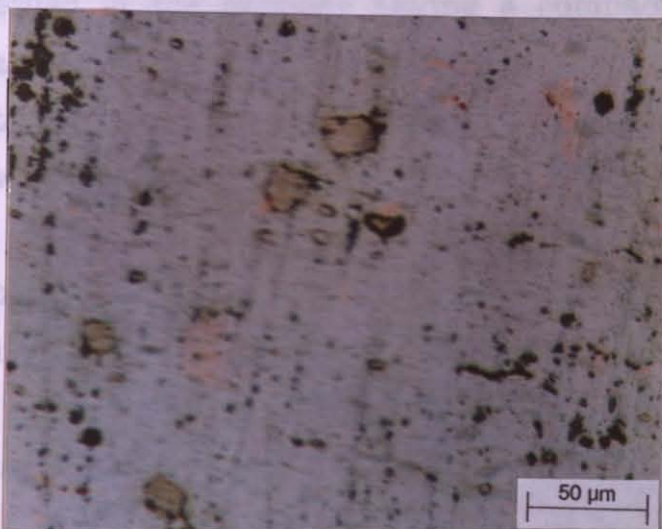


Fig. 4.12. Microstructure of the same specimen at the top part (1.5 cm from punch end) (x320).



Fig. 4.13. Microstructure at the same region of the Zn-Bi specimen squeeze cast under 85 MPa (x800, oil lens).

The segregation of bismuth particles especially, in the squeeze cast specimens is thought to be due to strain induced macrosegregation of the bismuth phase as observed during squeeze casting of Al-Si and Al-Mg systems before [31]. In these wide freezing range alloys the nucleated solid rejected the solute into the adjacent liquid. During punch closure enriched liquid was extruded up into the wall and rib areas of the casting. When the solidification was complete, steep solute remained in the part and resulted detrimental variations of mechanical properties within the part. This kind of macrosegregation was also observed in the castings having a compact geometry. The distinction was that the solute rich liquid was extruded out of the semisolid material into the hotter regions of the casting. When the solidification was complete, positive segregation remained in the part, located to the hot spot [31]. In the current study a similar mechanism was thought to work. Hence, after pouring the alloy into the die, the zinc-rich dendrites began to grow rejecting bismuth-rich liquid. As the pressure was applied, the remaining bismuth-rich liquid between the dendrite arms was also forced to move to the hotter regions. The solidification was completed under these conditions resulting a segregation of bismuth phase along the centerline of the casting especially near hot spot area. This event is diagrammatically illustrated in Fig. 4.14.

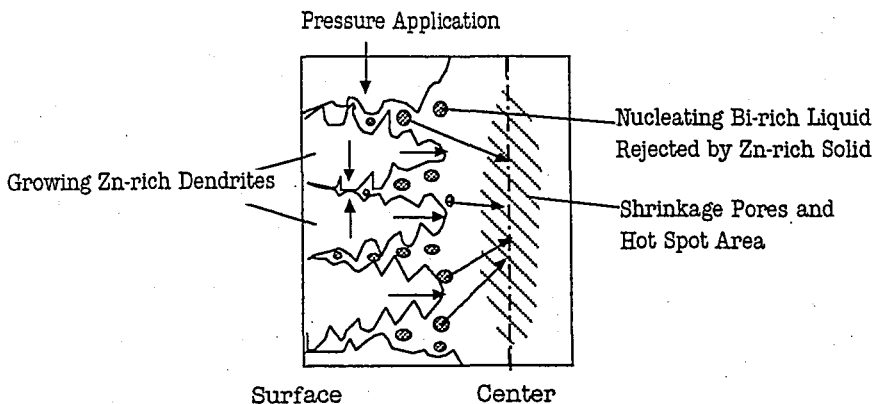


Fig. 4.14. Diagrammatic illustration proposed for the strain induced macrosegregation phenomena of Bi-rich phase in squeeze cast Zn-Bi monotectic alloy.

4.3 Chip Length Variation

Table 4.1. Average chip length vs alloy composition, squeezing pressure, die temperature and cutting speed.

When the chip lengths measured for pure zinc and Zn-Bi alloy were compared, it was clear that the addition of bismuth significantly improved the machinability (i.e. chip disposal) of zinc. In Fig. 4.15 the chips obtained from machining of squeezed and not-squeezed pure zinc and Zn-Bi monotectic specimens are shown. Where the average chip length was varied from 36 to 1070 mm for pure zinc castings under various cutting speeds, the chip lengths were reduced to 17 to 28 mm for Zn-Bi monotectic alloy squeeze cast under different pressures and then, turned under different cutting speeds. As the squeezing pressure was increased average chip length was decreased, i.e. machinability increased in all groups. Table 4.1 shows the average chip lengths for all groups at four different cutting speeds and, Fig. 4.16 shows the variation of chip length of Zn-Bi monotectic alloy with pressure at a fixed cutting speed of $V = 23.4$ m/min.

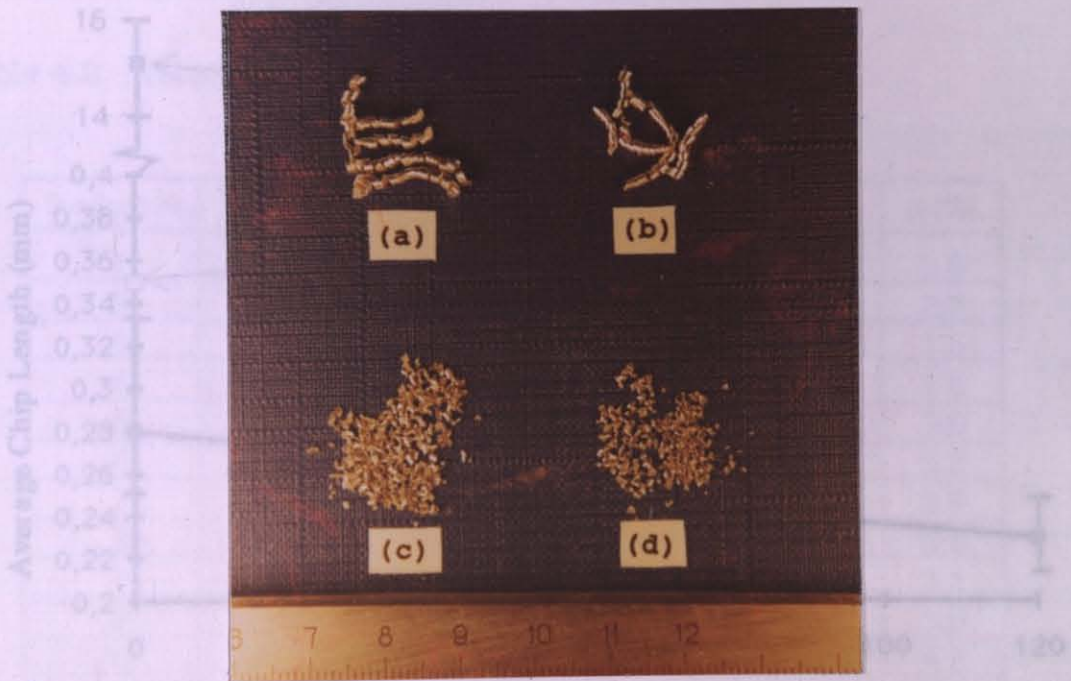


Fig. 4.15. Chips obtained from; (a) pure zinc not-squeezed, (b) pure zinc squeezed under 120 MPa, (c) Zn-Bi not-squeezed, (d) Zn-Bi squeezed under 120 MPa, castings at a cutting speed of 69 m/min.

Table 4.1. Average chip length vs alloy composition, squeezing pressure, die temperature and cutting speed.

ALLOY	P(MPa)	AVERAGE CHIP LENGTH (cm)			
		V=24,5m/min	34,5m/min	48,3 m/min	69m/min
99.95%	Atm. T(die)=400 °C	107	95	112	59
Pure Zn	120 T(die)=400 °C	15.1	9	3.6	3.6
Zn-1.9%Bi	Atm. (cold die) T(die)=20 °C	0,35	0,28	0,21	0,23
	Atm. (hot die) T(die)=250 °C	0,28	0,21	0,22	0,17
	50	0,26	0,27	0,20	0,25
	85	0,24	0,23	0,21	0,20
	120	0,23	0,23	0,22	0,17

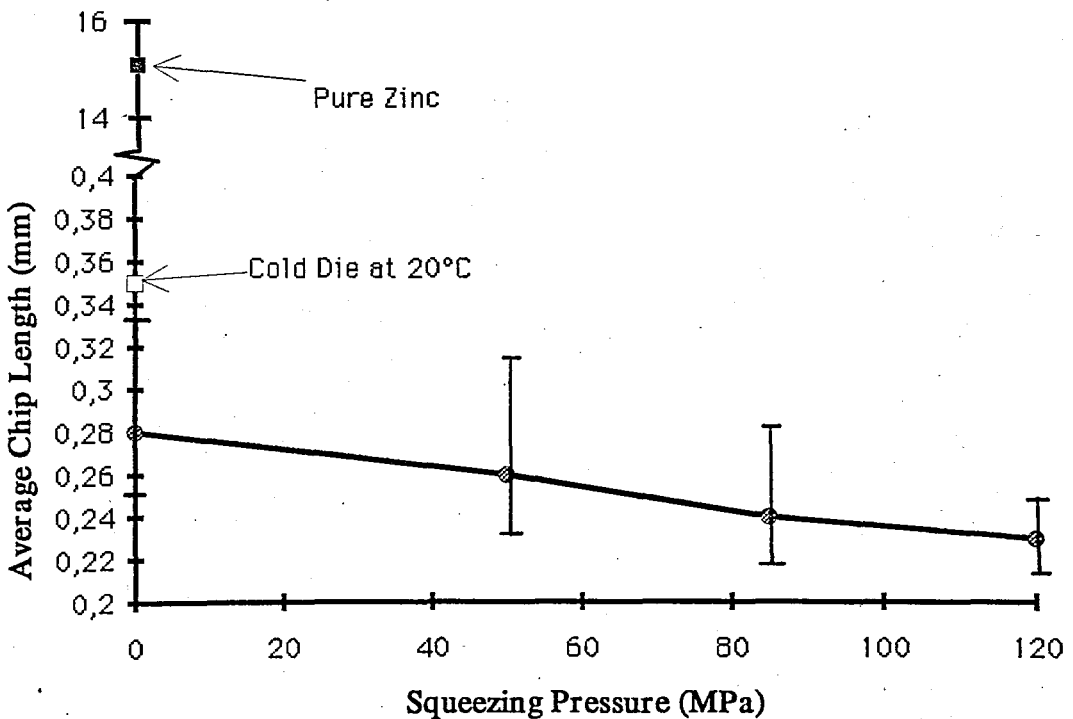


Fig. 4.16. The variation of average chip length in Zn-Bi monotectic alloy with squeezing pressure at a cutting speed of V=24,5 m/min.

4.4 Tensile Properties

Tensile test results of the fractured specimens are given in Table 4.2. The table includes 0.2% offset yield strength (σ_y), fracture strength (σ_f) and elongation at fracture (ϵ_f) values for all seven groups of the Zn-Bi monotectic alloy and also pure zinc castings. Among the not-squeezed specimens Group 1 (cold die) appeared to have a higher tensile strength than Group 2 (hot die) specimens. Squeeze cast specimens gave better results than not-squeezed specimens but, there was no clear improvement recorded with increasing pressure. During the tension tests, for all the specimens it was observed that the crack initiated at the inside and central part of the specimens where the coarser bismuth particles and central shrinkage piping were concentrated. The existence of coarser bismuth particles also verified in microstructural examination. The variation of tensile strength with squeezing pressure is shown in Fig. 4.17.

Table 4.2. Tension test data.

Specimen No.	Pressure (MPa)	Die Temp. (°C)	σ_y (MPa)	σ_f (MPa)	ϵ_f (%)
1	0	20	8.5	23.5	2.6
2	0	20	11.1	29.3	2.8
3	0	250	12.4	16.5	1.5
4	0	250	12.0	20.8	1.8
5	50	250	8.0	24.0	3.6
6	50	250	9.0	36.5	5.3
7	85	250	13.7	29.8	2.9
8	85	250	8.6	29.5	3.4
9	120	250	8.5	27.5	3.1
10	120	250	8.9	31.1	3.6
11	0 Pure Zn	400	8.4	31.5	4.6
12	120 Pure Zn	400	4.9	33.7	5.4
13	120 Pure Zn	400	5.7	34.1	5.3
14	120 Pure Zn	400	6.6	48.6	6.4

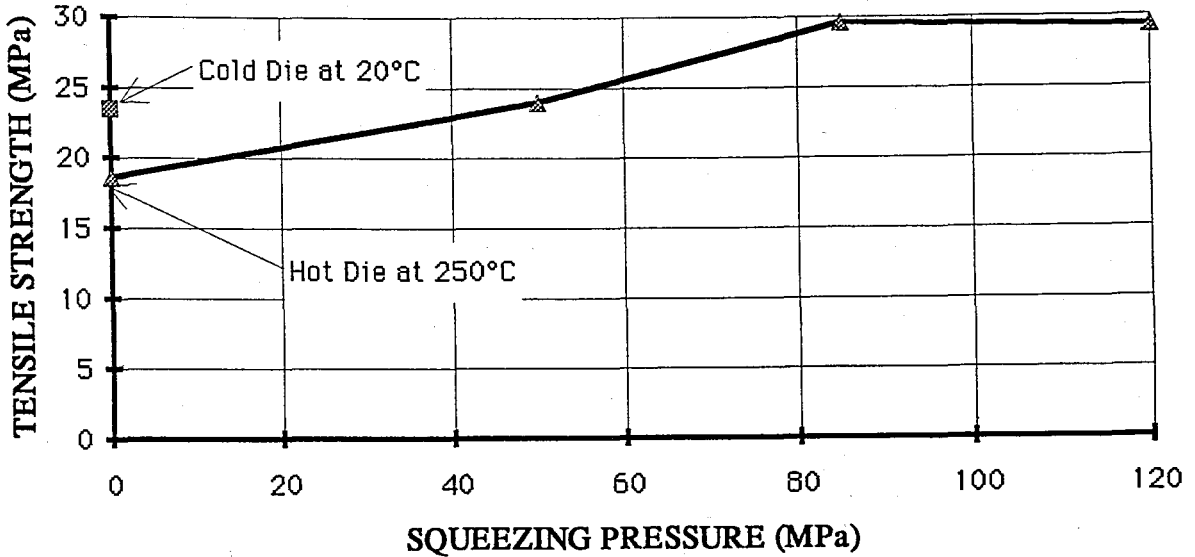


Fig. 4.17. The variation of tensile strength with squeezing pressure.

No clear relation was observed between porosity content and tensile strength. Group 2 (not-squeezed, hot die) specimens were denser than Group 1 (not-squeezed, cold die) specimens but, showed a lower strength. And, for the squeeze cast groups the porosity amount was decreased as the pressure increased but, no clear increase was observed in tensile strengths. The apparent densities and porosities calculated for the specimens are shown in Table 4.3 and the variations of porosity content and density versus squeezing pressure are plotted in Fig. 4.18.

Table 4.3. Apparent densities and porosity contents calculated in the tension test specimens.

Specimen No.	Pressure (MPa)	Die Temp.(°C)	Density (g/cm ³)	Porosity (%)
1	0	20	7.07	1.46
2	0	20	7.13	0.64
3	0	250	7.17	0.10
4	0	250	7.15	0.40
5	50	250	7.11	1.03
6	50	250	7.13	0.72
7	85	250	7.14	0.60
8	85	250	7.15	0.42
9	120	250	7.17	0.08
10	120	250	7.16	0.25

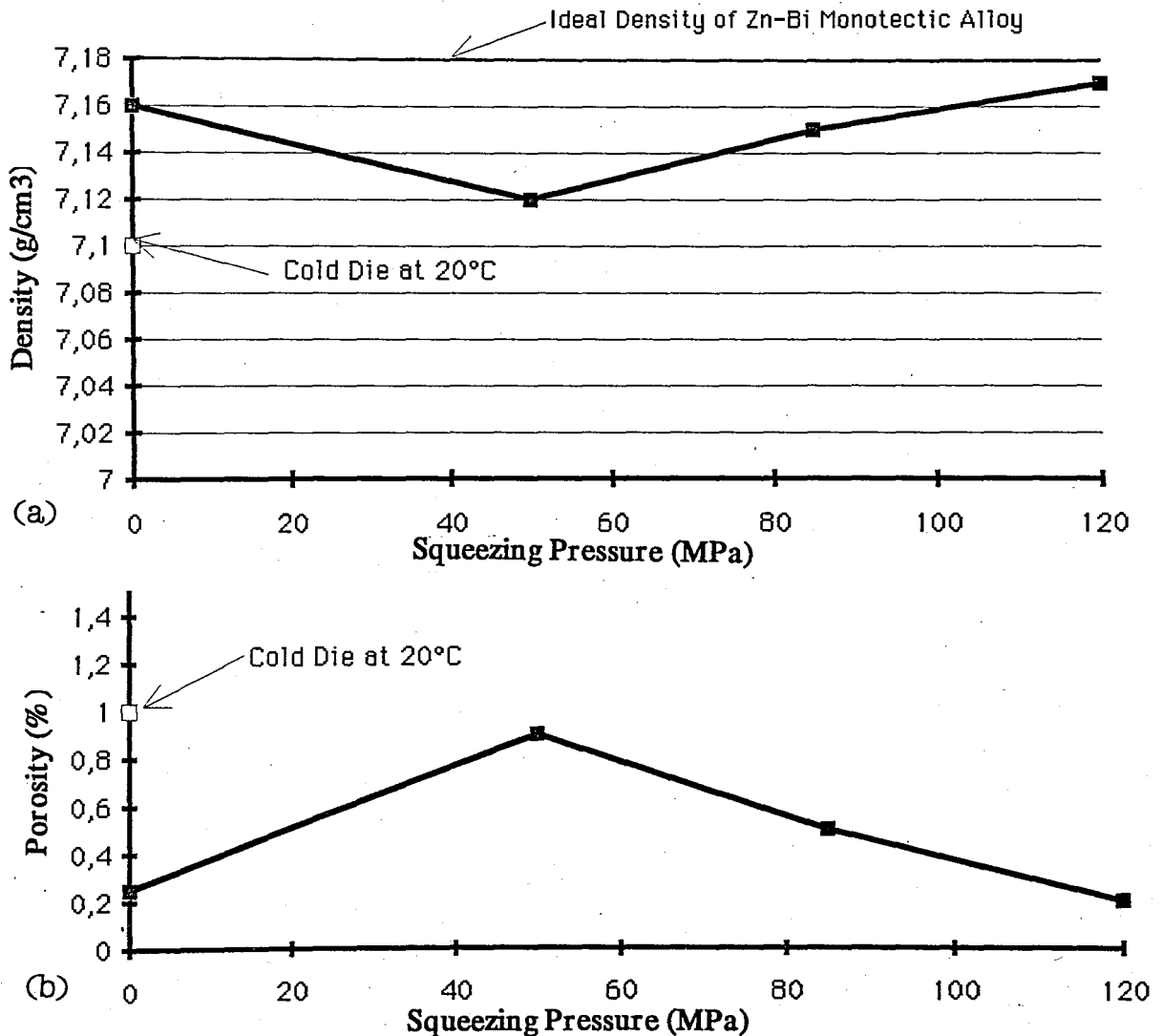


Fig. 4.18. Effect of squeezing pressure on (a) density, (b) porosity levels.

The values of yield strength (σ_y), fracture strength (σ_f), elongation at fracture (ϵ_f), obtained in this work and in directional solidification experiments of the Zn-Bi alloy [35] are tabulated in Table 4.4 for a comparison. As can be seen from this table, the directionally grown specimens of the optimum growth rate has shown twice the tensile strength obtained for the specimens squeeze cast at 120 MPa.

Table 4.4. Tensile properties of gravity cast, squeeze cast and directionally solidified Zn-Bi monotectic alloy.

Casting Condition	σ_y (MPa)	σ_f (MPa)	ϵ_f (%)
Gravity Cast (T die=20°C)	9.8	26.6	2.7
Gravity Cast (Tdie=250°C)	12.2	18.7	1.7
Squeeze Cast (50 MPa)	8.5	26.0	4.5
Squeeze Cast (85 MPa)	11.2	29.9	3.2
Squeeze Cast (120 MPa)	8.7	29.8	3.3
Dirac. Grown (8.6 cm/h)	25	32.5	2.02
Dirac. Grown (4.7 cm/h)	23	55	4.9

4.5. Hardness Variation

Average Vickers Hardness values obtained from the measurements on six specimens are given in Table 4.5.

Table 4.5. Average Vickers Hardness (H_V) values of the specimens

<u>Specimen</u>	<u>Average Hardness(H_V)</u>
Pure zinc	38,9
Not squeezed-Cold die	37,5
Not-squeezed-Hot die	38,3
Squeezed-50 MPa	38
Squeezed-85 MPa	40,5
Squeezed-120 MPa	40,8

The Vickers Hardness values of the Zn-Bi specimens varied both along longitudinal and radial directions. Along the centerline of the casting the hardness values were higher near the punch end and the bottom of the specimen but, along the line parallel to the centerline and 4 mm away from the surface no clear change in hardness values were observed. In the radial direction the maximum hardness values were measured midway between the centerline and the casting surface. In Fig. 4.19 the variation of hardness along the longitudinal axis of specimens and in Fig. 4.20 the variation of hardness in radial direction of the specimen squeeze cast at 120 MPa are shown.

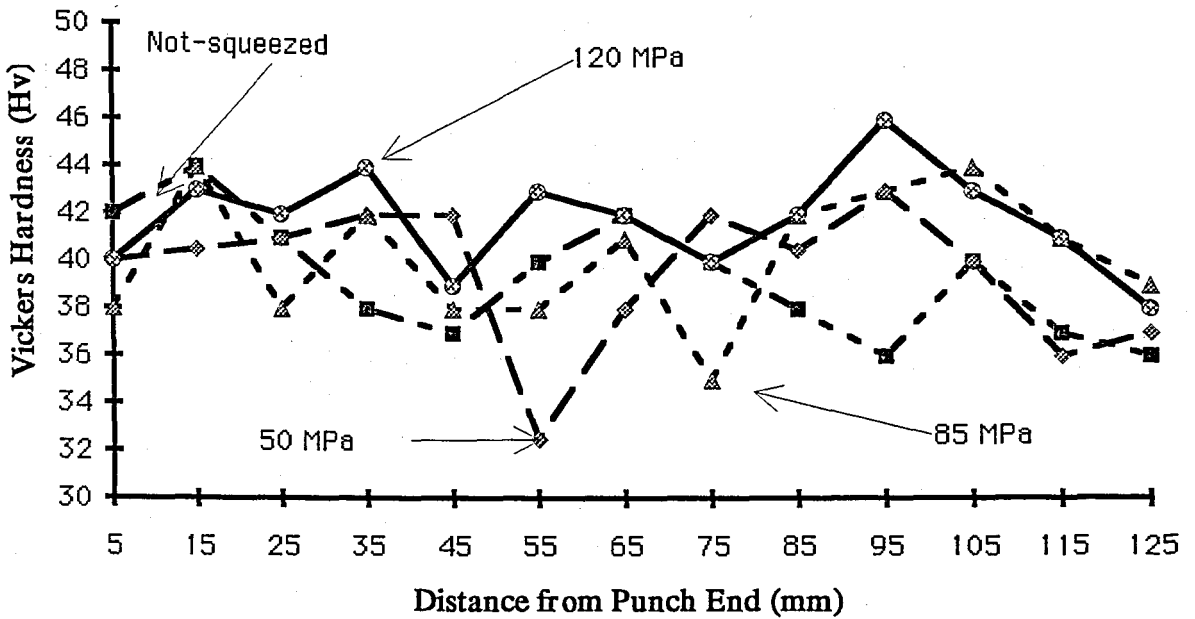


Fig. 4.19. Variation of Vickers Hardness in Zn-Bi monotectic specimens along centerlines of the specimens.

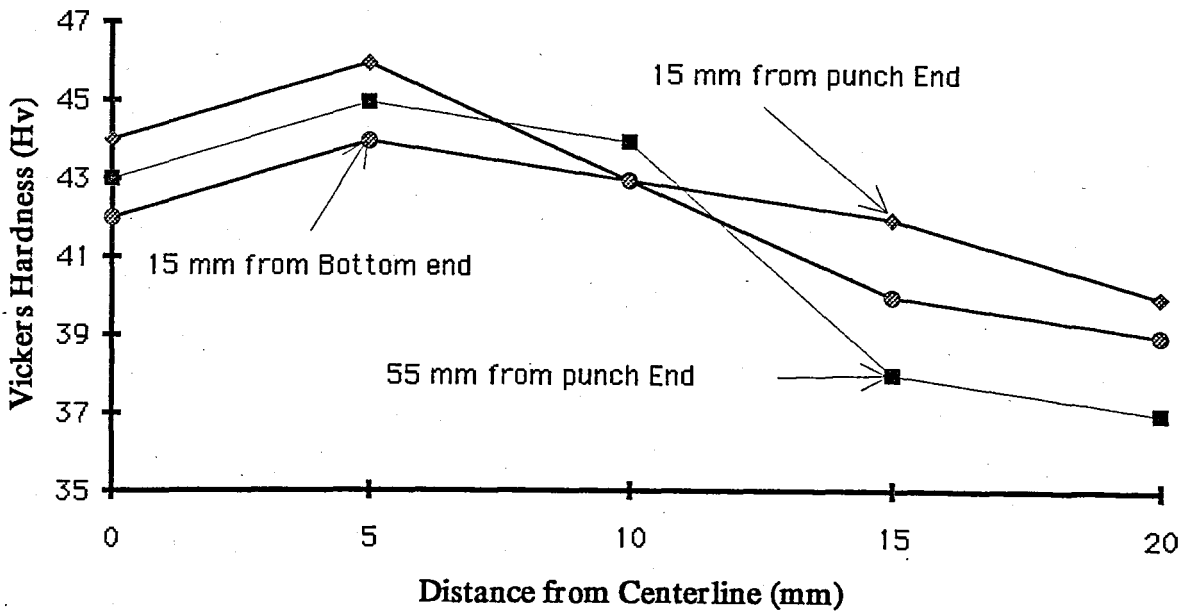
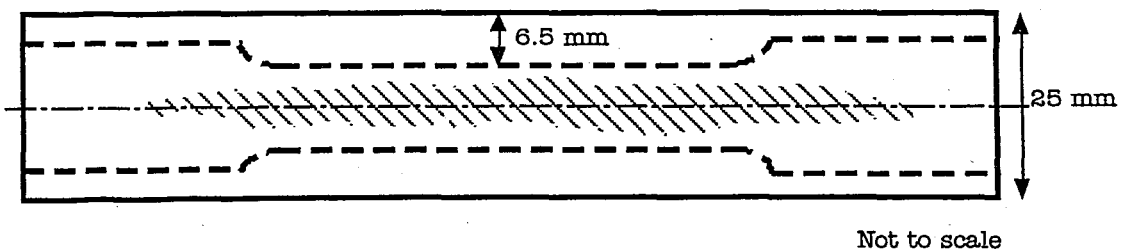


Fig. 4.20. Variation of hardness in the radial direction of the specimen squeeze cast under 120 MPa.

4.6. Macro- and Microstructures vs Mechanical Properties

It was observed that as the squeezing pressure was increased the amount of porosity was decreased and, the tendency for strain induced macrosegregation was increased. It is thought that these two factors could counteract against each other and relax each other's effects. In the squeeze cast specimens as the pressure was increased the porosity content was decreased but macrosegregation therefore, concentration of bismuth-rich liquid especially in the central part and around hot spots were increased. During machining of tensile test specimens, 6.5 mm from the outer surface containing zinc-rich part of the specimens were removed. The removed part was expected to provide the ductility and strength of the specimen. After machining, the bismuth-rich part which is more brittle and has a lower strength than zinc-rich part was left at the center of the specimen. The relative position of the tension test specimen in the casting is illustrated in Fig. 4.21. As the squeezing pressure increased the bismuth amount at this region increased although, the porosity was decreased. As a result, no clear change in the tensile properties with the increasing pressure were recorded. In the directionally grown samples this phenomena was not observed due to homogenous distribution of bismuth particles along the radial direction [35].



- Casting
- - - - Tensile Test Specimen
- ////// Bi-rich Region

Fig. 4.21. The relative position of the tension test specimen in a typical casting.

In the macro- and microstructural examinations of squeeze cast samples it was also observed that the lower parts of the castings were solidified prior to application of pressure and therefore, did not experienced the effects of pressure. So, variations in the mechanical properties along the longitudinal axis were expected mainly due to this fact and, also due to gravitational segregation of the phases. From microstructural examinations and hardness tests gravitational segregation was expected to be a more dominant factor in the not-squeezed hot-die castings.

The variation in the distribution of bismuth particles and porosity level were found to counteract also in the hardness tests. The bismuth-rich central part was expected to have a higher hardness but due to high porosity level in this part the hardness values were observed to be lower than the hardness values of the region between centerline and the edge. The punch end regions of the squeeze cast samples showed the highest hardness values along the specimen due to lower porosity level as a result of pressurized fast cooling.

V. CONCLUSIONS

In the present study, the mechanical properties, macro- and microstructures of the Zn-Bi monotectic alloy cast under different squeezing pressures were examined. The main conclusions derived from this study can be summarized as follows:

1. From the cooling curve measurements it was clearly seen that the freezing time of the squeeze cast specimens were significantly shorter than the freezing time of the not-squeezed specimens.
2. Central piping was found in all specimens. This was reduced in size with increasing pressure. In addition, the total porosity level decreased with increasing squeezing pressure.
3. The finest grains were found in the sample that has been cast into cold die. As the die temperature was increased the average grain size was increased but, with increased squeezing pressure the average grain size was decreased especially near the punch end.
4. In the not-squeezed specimens as the temperature was increased, the bismuth phase was observed to segregate to the bottom portion due to gravitational segregation. In the squeeze cast specimens the bismuth phase was observed to segregate along the centerline of the specimen due to strain induced macrosegregation.
5. The machinability of zinc was improved significantly after bismuth addition. Also, both in the pure zinc and Zn-Bi monotectic castings the machinability was increased as the squeezing pressure was increased.

6. The overall and local hardness values of the castings were influenced by the counteracting behavior of both the porosity level and bismuth phase distribution. As the squeezing pressure was increased porosity level was decreased but, segregation of phases increased. In the hardness tests, central part of the squeezed specimens were found to have a lower hardness, although it was rich in harder bismuth phase. This was because of the high porosity content.

7. The same tendency was observed also in tensile tests. In the squeeze cast specimens, although the porosity level was decreased no clear increase in tensile strength was observed. This is thought to be due to the fact that, while machining the tensile test specimens the zinc-rich outer part (skin), which was more ductile and had a higher strength, was removed. This left the bismuth-rich part of the center of a casting which had a lower tensile strength and was more brittle.

8. The microstructures of the specimens were also inhomogeneous in the longitudinal direction. In the not-squeezed specimens this fact was thought to be due to the gravitational segregation of the bismuth rich liquid. In the squeeze cast specimens gravitational segregation was not seem to be a major factor and, it was thought to be due to solidification of lower parts of the casting before pressure application.

VI. RECOMMENDATIONS FOR FUTURE WORK

1. A new die, which is designed to produce castings directly for tension test, will eliminate the effects of machining on tensile properties. Since, the die temperature is one of the most important parameters, a temperature monitoring facility for the die will be helpful to control the die temperature more closely.
2. A chemical analysis along a sample to reveal the bismuth content at any location and its comparison with hardness test results is recommended for future work. This will also help to assess the effect of porosity more clearly.
3. A more detailed and quantitative microstructural analysis should be performed. For instance; volume fraction, distribution, spacing and size of both bismuth particles and also porosity should be found.
4. The examination of the fracture surfaces of tension test samples under SEM (Scanning Electron Microscope) will reveal the fracture behaviors.

VII. REFERENCES

1. Grugel, R.N., and Hellawell, A., "Alloy Solidification in Systems Containing a Liquid Miscibility Gap", *Metallurgical Transactions*, Vol.12A, pp.669-681, 1981.
2. Kamio, A., Kumai, S., and Tezuka, H., "Solidification Structure of Monotectic Alloys", *Materials Science and Engineering*, Vol. A146, pp.105-121, 1991.
3. Andrews, J.B., Sandlin, A.C., and Curreri P.A., "Influence of Gravity Level and Interfacial Energies on Dispersion-Forming Tendencies in Hypermonotectic Cu-Pb-Al Alloys", *Metallurgical Transactions*, Vol. 19A, pp.2645-2650, 1988.
4. Shah, S., Grugel, R.N., and Lichter, B.D., "Directional Solidification of Lead-Copper Immiscible Alloys in a Cyclic Gravity Environment", *Metallurgical Transactions*, Vol.19A, pp.2677-2680,1988.
5. Dhindhaw, B.K., Stefanescu, D.M., Singh, A.K., and Curreri, P.A., "Directional Solidification of Cu-Pb and Bi-Ga Monotectic Alloys Under Normal Gravity and During Parabolic Flight", *Metallurgical Transactions*, Vol.19A, pp. 2839-2846, 1988.
6. Carlberg, T., and Frederiksson, H., "The Influence of Microgravity on the Solidification of Zn-Bi Immiscible Alloys", *Metallurgical Transactions*, Vol.11A, pp.1665-1676, 1980.
7. Zhang, Z., Long, s., and Flower, H.M., "Light Alloy Composite Production by Liquid Metal Infiltration", *Composites*, Vol. 25, pp.380-392, 1994.
8. Kang, H.G., Zhang, D.L., and Cantor, B., "The Microstructures of Locally Reinforced Squeeze-cast Al-alloy Metal-matrix Composites", *Journal of Microscopy*, Vol. 169, pp.239-245, 1993.

9. Fukunaga, H., Komatsu, S., and Kanoh, Y., "The Production-scale Squeeze Casting of Devitroceramic Fiber Reinforced Aluminum and its Mechanical Properties", *Bulletin of the JSME*, Vol.26, pp.1814-1819, 1983.
10. Fukunaga, H., and Kuriyama, M., "Experimental Study on the Fabrication of Fiber Reinforced Aluminum by Squeeze Casting", *Bulletin of the JSME*, Vol.25, pp.842-847, 1982.
11. Rajagopal, S. , "Squeeze Casting: A Review and Update", *Journal of Applied Metalworking*, Vol. 1, pp. 3-14, 1981.
12. Okada, S., Fujii, N., Goto, A., Moritomo, S., and Yasuda T., "Development of a Fully Automatic Squeeze Casting Machine", *AFS Transactions*, Vol.16, pp.135-146,1982.
13. Kulkarni, K.M., Stawartz, D., and Mielot, R.B., "Feasibility of Squeeze Casting Ferrous Components", *Fourth North American Metalworking Research Conference*, Ohio, pp.58-66, 1976.
14. Savaş, M.A. and Altıntaş, S., "Effects of Squeeze Casting on Wide Freezing Range Binary Alloys", *Materials Science and Engineering*, Vol. A173, pp.227-231, 1993.
15. Chadwick, G.A., and Yue, T.M., "Principles and Applications of Squeeze Casting", *Metals and Materials*, Vol. 5, pp.5-12, Jan. 1989.
16. Kulkarni, K.M., "Hybrid Processes Combine Casting and Forging", *Machine Design*, Vol.46 (11), pp.125-128, May 1974.
17. Gethin, D.T., Lewis, R.W., and Tadayon, M.R., "A Finite Element Approach for Modeling Metal Flow and Pressurized Solidification in the Squeeze Casting Process", *International Journal for Numerical Methods in Engineering*", Vol.35, pp.939-950,1992.
18. Chadwick G.A., "Squeeze Casting of Metal Matrix Composites Using Short Fibre Preforms", *Materials Science and Engineering*, A135, pp.23-28, 1991.
19. Mortensen, A., and Cornie, J.A., "On the Infiltration of Metal Matrix Composites", *Metallurgical Transactions*, Vol. 18A, pp.1160-1163, 1987.

20. El Mahallawy, N.A., Taha, M.A., and Zamzam, M.L., "On the Microstructure and Mechanical Properties of Squeeze Cast Al-7wt%Si Alloy", *Journal of Materials Processing Technology*, Vol.40, pp.73-85,1994.
21. Chadwick, G.A., **Metallography of Phase Transformations**, NewYork, Crane and Russak, pp.152-159, 1971.
22. Uhlmann, D.R., Chalmers, B., and Jackson, K.A., "Interaction Between Particles and a Solid-Liquid Interface", *Journal of Applied Physics*, Vol. 35, pp.2986-2993, 1964.
23. Cahn, J.W., "Monotectic Composite Growth", *Metallurgical Transactions*, Vol. 10A, pp. 119-121, 1979.
24. Toloui, B., Macleod, A.J., and Double, D.D., "Microstructural Perturbations in Directionally Solidified Al-In, Al-Bi and Zn-Bi Monotectic Alloys", *In-Situ Composites IV*, Elsevier Science Publishing, pp.153-266, 1982.
25. Chadwick, G.A., "Monotectic Solidification", *British Journal of Applied Physics*, Vol16, pp.1095-1097, 1965.
26. Livingstone, J.D., and Cline, H.E., "Monotectic Solidification of Cu-Pb Alloys", *Transactions of the Metallurgical Society of AIME*, Vol.245, pp.351-357, 1969.
27. Kim, S., Lichter, B.D., and Grugel, R.N., "Application of Directionally Solidified Pb-Cu Alloys", *30th Annual Conference of Metallurgists (poster)*, Ottawa, 1991.
28. Goswami, R., and Chattopadhyay, K., "Microstructural Evolution and Transformation Pathways in the Near Monotectic Zn-rich Zn-Bi Alloys During Rapid Solidification", *Acta Metall. Mater.*, Vol.42, pp.383-393, 1994.
29. Smith, S.J. Ed., **Metals Reference Book**, 5th ed., pp.396-752, Butterworth, London, 1976.
30. Epanchintsev, O.G., "Structure and Properties of Metals Solidified at High Pressures" (abstract), *Russian Casting Production*, Jan. , pp. 34-37, 1972.

31. Rolland, T., Flatval, R., and Arnberg, L., "Strain Induced Macroseggregation in Squeeze Cast Al-Mg and Al-Si Alloys", *Materials Science and Engineering*, Vol. A173, pp.267-270, 1993.
32. ASTM Standards-1985, B557M, Vol.03.01, pp.94.
33. ASTM Standards-1985, D792A.
34. Smith, S.J. Ed., **Metals Reference Book**, 5th ed., pp.292,293, Butterworth, London, 1976.
35. Şimşek, E., "Microstructure and Mechanical Properties of Unidirectionally Solidified Zn-Bi Monotectic Alloy", M.S. Thesis, Boğaziçi University, 1994.